The effect of the flame phase on thermoacoustic instabilities

G. Ghirardo[a,*], M.P. Juniper[b], M.R. Bothien[a]

[a]*Ansaldo Energia Switzerland, Baden 5401, CH*
[b]*University of Cambridge, Cambridge CB2 1PZ, UK*

Abstract

This paper concerns the influence of the phase of the heat release response on thermoacoustic systems. We focus on one pair of degenerate azimuthal acoustic modes, with frequency ω_0. The same results apply for an axial acoustic mode. We show how the value ϕ_0 and the slope $-\tau$ of the flame phase at the frequency ω_0 affects the boundary of stability, the frequency and amplitude of oscillation, and the phase ϕ_{qp} between heat release rate and acoustic pressure. This effect depends on ϕ_0 and on the nondimensional number $\tau\omega_0$, which can be quickly calculated. We find for example that systems with large values of $\tau\omega_0$ are more prone to oscillate, i.e. they are more likely to have larger growth rates, and that at very large values of $\tau\omega_0$ the value ϕ_0 of the flame phase at ω_0 does not play a role in determining the system's stability. Moreover for a fixed flame gain, a flame whose phase changes rapidly with frequency is more likely to excite an acoustic mode.

We propose ranges for typical values of nondimensional acoustic damping rates, frequency shifts and growth rates based on a literature review. We study the system in the nonlinear regime by applying the method of averaging and of multiple scales. We show how to account in the time domain for a varying frequency of oscillation as a function of amplitude, and validate these results with extensive numerical simulations for the parameters in the proposed ranges. We show that the frequency of oscillation ω_B and the flame phase ϕ_{qp} at the limit cycle match the respective values on the boundary of stability. We find good agreement between the model and thermoacoustic experiments, both in terms of the ratio ω_B/ω_0 and of the phase ϕ_{qp}, and provide an interpretation of the transition between different thermoacoustic states of an experiment. We discuss the effect of neglecting the component of heat release rate not in phase with the pressure p as assumed in previous studies. We show that this component should not be neglected when making a prediction of the system's stability and amplitudes, but we present some evidence that it may be neglected when identifying a system that is unstable and is already oscillating

Keywords: Thermoacoustic stability; phase response; flame phase; delayed differential equations

Nomenclature

′	the prime denotes time derivative of the preceding quantity
ˆ	the hat denotes the Fourier transform of the underlying quantity
p	acoustic pressure, suitably nondimensionalized
u	acoustic velocity in the azimuthal direction, suitably nondimensionalized
u_{ax}	acoustic velocity in the axial direction, typically long the axis of the burner, suitably nondimensionalized
q	fluctuating heat release rate, suitably nondimensionalized, often called flame response
$Q(A,\omega)$	describing function of the fluctuating heat release rate $q = q[p]$ as function of p. Defined in (3)
A_j	slowly varying amplitudes of oscillations, introduced in (29)

n	azimuthal order of the mode, e.g. $n = 3$ refers to the third azimuthal
α	equivalent acoustic damping coefficient, appearing in (7b)
β	flame strength, i.e. the nondimensional linear flame response gain as function of p, as in $|q| \propto \beta|p|$
γ_k	standard deviation of the k-th time delay, see (12), appearing also in Fig. 4
δ	nonlinear saturation coeff. as in (37a)
$\eta_j n$	amplitudes of the azimuthal acoustic velocity of the 2 modes as in (8), for $j = 1, 2$
η_j'	amplitudes of the acoustic pressure of the 2 modes as in (8), for $j = 1, 2$
θ	azimuthal coordinate along the annular combustion chamber, $\theta \in [0, 2\pi)$
κ	nonlinear saturation coefficient, appearing in (16)
λ	eigenvalue, $\lambda = \sigma + i\omega$, with ω in rad/s
μ	L2 norm of the mode, as defined in (11)
ν	expression for the growth rate appearing in (38)
σ	growth rate, i.e. real part of the eigenvalue $\lambda = \sigma + i\omega$

*Corresponding author
Email address:* giulio.ghirardo@ansaldoenergia.com (G. Ghirardo)

$-\tau\omega_0$ Nondimensional slope of the flame phase in the vicinity of the acoustic mode with frequency ω_0

τ equivalent time delay of the transfer function $\hat{q}/\hat{p}$ as introduced in (15), i.e. minus the local slope of of the flame phase of such transfer function at frequencies close to ω_0.

$\phi(\omega)$ flame phase response, i.e. the argument of Q, as function of the frequency ω. We assume that it does not depend on the amplitude of oscillation A. This quantity depends on the geometry upstream of the flame and on the flame response.

ϕ_0 flame phase at the acoustic frequency $\omega = \omega_0$, i.e. $\phi(\omega_0)$

ϕ_{qp} phase between q and p of a thermoacoustic mode at frequency ω_B, i.e. $\phi(\omega_B)$

φ_j slowly varying phase of the j-th azimuthal mode, $j = 1, 2$

φ slowly varying phase difference $\varphi_1 - \varphi_2$ of the two azimuthal mode

χ radial and axial shape of the azimuthal modes, $\chi(r, z)$

ω angular frequency, variable

ω_0 angular **acoustic** frequency of oscillation when the flame and the damping are virtually shut off and the system becomes conservative. This is the frequency of oscillation of the acoustic mode without being excited by the flame and without being damped by the acoustic losses

ω_B angular **thermoacoustic** frequency of the system if the flame response gain β is virtually decreased until the system is neutrally stable, i.e. the growth rate σ becomes zero, solution of (27). We prove that ω_B is also the frequency of the limit-cycle solution if the flame phase does not depend on the amplitude and the damping losses are linear, as is the case in this work

ω_{LC} angular frequency of oscillation at the limit cycle, proved to match ω_B

Ω Domain of the combustor

1. Introduction

We first review fundamentals of thermoacoustic instabilities in §1.1 and present three key questions on the subject, then review the existing literature in §1.2, and briefly outline the paper in §1.3.

1.1. Motivation of this work

Rayleigh [1] was the first to observe that if part of the fluctuating heat release rate q is in phase with the acoustic pressure p self sustained acoustic oscillations can occur. Accounting also for acoustic losses [2, 3], considering the case of a single acoustically compact flame and assuming a low Mach number flow, the criterion requires that

$$\frac{1}{T}\int_t^{t+T} q(t)p(t)dt > \quad \begin{array}{l}\text{acoustic}\\\text{losses}\end{array} \tag{1}$$

where $T = 2\pi/\omega$ is the period of the thermoacoustic instability and ω its angular frequency, q and p are considered at the flame location, and we assume thermodynamic equilibrium and a perfect gas. Under suitable assumptions discussed later, one can express[1] the fluctuating heat release rate as function of the pressure p as $q = \mathcal{Q}[p]$. For the sake of brevity, in the following we will often refer to q as the flame response to the pressure p, or simply as the flame response. We assume and substitute a sinusoidal pressure $p(t) = A\cos(\omega t)$ in (1):

$$\frac{1}{T}\int_t^{t+T} \mathcal{Q}[A\cos(\omega t)]A\cos(\omega t)dt > \quad \begin{array}{l}\text{acoustic}\\\text{losses}\end{array} \tag{2}$$

We now define the describing function $Q(A, \omega)$ of an operator $\mathcal{Q}$ of a sinusoidal input at frequency ω and with an amplitude A similarly to [4]:

$$Q(A, \omega) \equiv \frac{1}{A}\frac{2}{T}\int_t^{t+T} \mathcal{Q}[A\cos(\omega t)]e^{-i\omega t}dt \tag{3}$$

We multiply and divide the left hand side of (2) by $2/A^2$, and by substituting the real part of (3) we obtain

$$\frac{1}{2}\text{Re}[Q(A, \omega)]A^2 > \quad \begin{array}{l}\text{acoustic}\\\text{losses}\end{array} \tag{4}$$

On the left hand side, we recover the typical structure of a conservative potential; for example, for a linear spring with constant k loaded with a steady displacement A, the energy is $kA^2/2$, where the describing function is real valued, does not depend on the amplitude A because the spring is linear and matches the constant k. We can rewrite the complex valued describing function in terms of its real valued, non-negative gain G and real valued phase response ϕ:

$$Q(A, \omega) = G(A, \omega)e^{i\phi(A, \omega)} \tag{5}$$

In the following we will refer for brevity to G as flame gain and to ϕ as flame phase. By substituting (5) in (1) we obtain:

$$\frac{1}{2}G(A, \omega)\cos\left(\phi(A, \omega)\right)A^2 > \quad \begin{array}{l}\text{acoustic}\\\text{losses}\end{array} \tag{6}$$

Equation (6) allows the same interpretation of (1), but in terms of the flame gain G and flame phase ϕ of the describing function Q. We then review known results discussed first by [1]. We observe that the acoustic loss term on the right hand side of (6) is positive, so that in order for (4) to hold we require that $\cos(\phi) > 0$, i.e. that $-\pi/2 < \phi(A, \omega) < \pi/2$. Once this first

---

[1]with the exception of the trivial cases where the flame is located at a pressure node of the acoustic field at frequency ω. These cases cannot be unstable because the left hand side of (1) is zero.

necessary condition is satisfied, there exists a threshold value of the gain above which (4) is verified and a thermoacoustic oscillation ensues.

This perspective in terms of an acoustic energy balance correctly captures the dominant feature of the thermoacoustic problem as a self excited closed loop system, which in an enclosed cavity has a set of countable thermoacoustic eigenmodes. We can interpret the Rayleigh criterion at the frequency ω of the nonlinearly saturated eigenmode at a limit cycle, i.e. at the dominant frequency peak of a thermoacoustically unstable experiment. We distinguish ω from the eigenfrequency ω_0 of the acoustic mode of the combustor obtained when a passive flame is considered. We now consider three other scenarios, where the Rayleigh criterion does not allow us to conclude much.

1. We consider a thermoacoustic system with an acoustic mode at frequency ω_0, with a flame phase that in the linear regime is[2] $\phi(\omega_0) = -\pi$. We can conclude based on the analysis above that the system cannot pulsate at the frequency ω_0. However, the acoustic mode could shift to a frequency $\omega_0 + \Delta\omega$ such that the phase $\phi(\omega_0 + \Delta\omega)$ becomes favourable for the instability. Under what conditions does this happen? Which nondimensional numbers characterizing the flame response govern this?

2. We consider a given thermoacoustic system that is pulsating at large amplitudes at a frequency ω. What would happen[3] if — as a pulsation mitigation strategy — we could change the flame response so that the flame phase would be $\phi(\omega) + \pi$ instead of $\phi(\omega)$? Would this make the system stable without acoustic pulsations? Could the system instead exhibit pulsations at a perturbed frequency of oscillation $\omega + \Delta\omega$ such that the phase $\phi(\omega + \Delta\omega)$ would still be favourable for pulsations?

3. We consider two flames characterized by two different transfer/describing functions, and predict what happens when they are placed one at a time in a hypothetical combustor with a given set of random (but physical) acoustic modes. Which features of the flame transfer function are most influential at provoking instability? We know already that large flame gains provoke instability but wish to examine the influence of the flame phase

We will refer to these three questions as the three scenarios in the following, and we will answer them as we unfold the problem. All three of them show how the Rayleigh criterion (1) or (6) is not sufficient to answer them. We will show that the missing piece of the puzzle is the imaginary part of the flame response $\text{Im}[Q(A, \omega)]$, which is the component of the fluctuating heat release q in quadrature with the pressure p. We review how this component is well known to be responsible for shifting the

frequency from the acoustic frequency ω_0 to the thermoacoustic frequency ω_B in the next subsection.

1.2. Literature review

All three scenarios can be tackled numerically for a specific combustor and flame response. In particular all the questions can be made more specific and quantitatively answered. We first discuss the methods, and review the results in the next paragraph. One can calculate the stability of a thermoacoustic system by coupling the acoustic field with the flame response and study the system both in the linear and nonlinear regime with respect to the amplitude of pulsation. See e.g. [5, 6, 7] for a finite element approach in the frequency domain, [8] in the time domain. Low order models can be analyzed in the frequency domain [9, 10, 11, 12, 13] and both in the frequency and time domain [14, 15, 16, 17]. These stability analyses allow the prediction of the frequencies and amplitudes of oscillation for a specific system [18], can account for subcritical bifurcations [19] and can be extended to quasi-periodic solutions [20]. However because the whole system behaviour depends first of all on the set of eigenmodes and eigenfrequencies of the system, which are specific to the geometry, it is hard to isolate the effect of the flame response on the system's stability when all the modes are considered. In particular when one changes the flame response, a new acoustic mode may be excited, or a competition of closely spaced eigenmodes can be observed. To isolate the effect of the flame response we focus here on one mode only or similarly on a couple of degenerate azimuthal modes.

Lang *et al.* [21] study a duct with a n-τ compact flame model with a wave-based approach, in terms of a linear dispersion relation. For $n = 0$ they calculate the acoustic frequency ω_0 of the system when the flame response is analytically switched off in the equations. They then apply a Maclaurin series truncated to the first order in the interaction index n to the dispersion relation to obtain an approximation of the thermoacoustic frequency ω in terms of the unperturbed frequency ω_0. Lang *et al.* [21] says: *When [the flame response is absent] the perturbation vanishes and the angular frequency is identical to one of the resonant frequencies of the duct.* Similarly also [22, eq. (50), Fig. 5] do not study the nondimensional numbers governing the system's stability, and present an approximate solution of the boundary of stability that does not account for the fact that the frequency of oscillation shifts from ω_0. Dowling & Stow [23, Fig. 2, eq. (21)] carry out a numerical sensitivity study of a n-τ model in a one dimensional duct, in terms of normalized frequency shifts and growth rates. The results are correct on a qualitative level, but the model does not account for damping losses, and the sensitivity is restricted to a small range of τ and for rather small levels of heat release rate response. Schuller *et al.* [24] also consider a n-τ model applied on the Helmholtz mode of one experiment. They assume that the frequency of oscillation is known, and apply the Rayleigh criterion to distinguish stable and unstable cases. A model similar to [24] is used by [25] to predict growth rates and frequencies of oscillation of one experiment at different operating conditions.

Although not written with this terminology, [21, 22, 23] show that the imaginary part $\text{Im}[Q(A, \omega)]$ of the flame describing

---

[2]for the sake of the examples we make the reasonable assumption that the gain saturates smoothly with amplitude, i.e. that the Hopf bifurcation is supercritical

[3]for the sake of the example we assume that no other thermoacoustic mode would be excited when ϕ is changed, and that ϕ does not depend on amplitude, as discussed later in §2.1

function — the part of the flame response that is in quadrature with the acoustic pressure p — is responsible for a frequency shift of the system from the acoustic frequency ω_0 to the thermoacoustic frequency ω_B. They show that the phase of the flame response introduced in (5) can make the system stable or unstable, as one can conclude from (6). This is for example apparent in [24, Fig. 10], and in [24, eq. (11)] where also acoustic losses are accounted for. They also typically consider the sensitivity of frequency and growth rate on the delay τ, see e.g. [23, Fig. 2], as is customary of many other studies, e.g. [8, 26, 27, 28, 29, 7]. The change of the delay affects at the same time the value and the slope of the flame phase at a certain frequency ω_0. It is then hard to pinpoint separately the role of the phase value and the role of the phase slope, which is one of the outcomes of this work.

We review in Table 1 selected references from the literature that discuss growth rates, damping rates and frequency shifts. These numbers allow us to quantify how weakly perturbed the thermoacoustic system is, i.e. how weakly the flame response and the acoustic losses are perturbing the acoustics of the problem. We observe that the thermoacoustic frequency ω_B can shift from ω_0 for approximately 10% of the value of ω_0, and that the nondimensional growth rate $|\sigma/\omega|$ is typically smaller than 0.1. Regarding the first column, we point out that strongly damped acoustic modes are not of interest in the applications because they tend to be very stable.

1.3. Outline

Our starting point is the work of [47, 48], who neglect the part of the flame response q that is not in phase with the acoustic pressure p, i.e. they consider only the real part of the transfer function $\mathrm{Re}[Q(A, \omega)]$. We instead maintain the complex transfer function $Q(A, \omega)$ so that we can discuss the role of the phase of this transfer function on the stability boundaries and on the nonlinear saturation of the system.

We limit the study to the more common case of a limit cycle solution, excluding for example quasi-periodic [49, 20] and chaotic [50, 51, 52] solutions that are beyond the limits of the model. We also neglect the study of intrinsic thermoacoustic modes [53, 54]. An important result of this work is that most results obtained on the linear boundary of stability are then also valid in the nonlinear regime at the limit cycle solution, allowing the practical usage of the results on self-excited thermoacoustic oscillations, under a set of assumptions regarding the flame response that are typically respected, discussed in §2.1.

The manuscript is organized as follows. In §2 we briefly characterize the problem, with a focus on the flame model. In §3 we carry out the linear analysis, and discuss the boundary of stability of the system. In §4 we extend the linear results to the nonlinear regime. We apply two analytical nonlinear methods to predict amplitudes and frequencies of the limit cycles. We validate them with extensive numerical simulations in the whole range of parameters explored. Results apply both to azimuthal and axial modes, and are discussed for azimuthal modes first and then extended to axial modes in §2.3 and §4.5. In §5 we discuss some implications of neglecting the part of

heat release rate not in phase with the pressure when identifying linear growth rates of a system. Finally in §6 we draw the conclusions.

2. Brief derivation of the model

Low-order models of azimuthal instabilities usually describe the system as a damped wave equation, with the fluctuating heat release rate q as a source term. The nondimensional equations are [48, 55]:

$$\frac{\partial u}{\partial t} + \nabla p = 0 \tag{7a}$$

$$\frac{\partial p}{\partial t} + \nabla u = q - \overline{\alpha}p \tag{7b}$$

In (7) $\overline{\alpha}$ is a positive damping coefficient, $p(t, \theta)$ is the fluctuating pressure, $u(t, \theta)$ is the fluctuating velocity in the azimuthal direction, with θ being the azimuthal angle in the periodic domain $[0\,,2\pi)$. The damping is modelled as linear because it is usually linear with respect to the amplitude, see e.g. [56], but one can account for an amplitude dependence, as discussed e.g. by [57] for the losses at the boundaries. We focus on a rotationally symmetric system in the azimuthal direction θ, i.e. we assume that u, p, q do not have any direct dependence on θ. A discussion of the effect of a discrete rotation group of symmetry, instead of full rotational symmetry, can be found in [44]. The discussion of the case covering the loss of degeneracy of the couple of eigenmodes is beyond the scope of this manuscript. This can occur for many reasons, e.g. a non uniform flame [58, 48] or damping [39] response or a non-zero mean azimuthal velocity [59, 60].

We approximate the solution of (7) with a superposition of the two excited degenerate thermoacoustic modes, which at the flames' positions have shapes $\cos(n\theta)\chi(r, z)$ and $\sin(n\theta)\chi(r, z)$, in a cylindrical coordinate system $\{r, z, \theta\}$ with the z axis as the axis of rotational symmetry of the combustor. We fix arbitrarily the value of the mode χ at the burners' radial and axial location to 1. At these $\{r, z\}$ coordinates the acoustic azimuthal velocity and pressure have the expressions

$$u(t, \theta) \approx n\eta_1(t)\sin(n\theta) - n\eta_2(t)\cos(n\theta) \tag{8a}$$

$$p(t, \theta) \approx \eta_1'(t)\cos(n\theta) + \eta_2'(t)\sin(n\theta) \tag{8b}$$

where here and in the following the prime denotes a time derivative and n is the azimuthal wavenumber of the mode we are studying. By substituting (8) into (7) and by projecting the equations on the two modes we obtain [44]:

$$\eta_1''(t) + \omega_0^2\eta_1(t) = \langle q \rangle_{\cos}(t) - \alpha\eta_1'(t) \tag{9a}$$

$$\eta_2''(t) + \omega_0^2\eta_2(t) = \langle q \rangle_{\sin}(t) - \alpha\eta_2'(t) \tag{9b}$$

where we introduce the spatial averaging operator for the generic function $m(\theta)$ as

$$\langle q \rangle_m(t) = \frac{1}{\pi\mu}\int_0^{2\pi} q(\theta, t)m(\theta)d\theta, \tag{10}$$

4

Table 1: List of values of damping/growth rates and frequency shifts from the literature. The references regard experiments or models tuned in some way to experimental data. This includes for example calculations with flame transfer functions evaluated with LES, thermoacoustic models tuned to experimental data or that use measured reflection coefficients, etc.. In this manuscript the eigenvalue is $\lambda = \sigma + i\omega$, where $f = \omega/2\pi$ is the frequency in Hz and σ is the growth rate. The acoustic frequency of oscillation is ω_0, and the thermoacoustic frequency of oscillation is ω_B. In each reference we collect the largest negative growth rates for the first column, largest positive growth rate for the second, and largest positive and negative shift from unity for the third column. This allows us later to discuss the boundaries of these parameters, rather than their common values. For the calculation of σ/ω_0 the approximation $\omega_B \approx \omega_0$ was made in the cases where ω_0 is not available

wo. flame σ/ω_0	w. flame σ/ω_0	ω_B/ω_0	Reference and brief description
		1.114	From Bloxsidge *et al.* [2], experiment. Freq. shift observed when the controller is switched on from an unstable point, stabilizing the system
-0.128 -0.052 -0.026			From Moeck *et al.* [19, Table 1], experiment
	0.039	0.968	From Noiray *et al.* [30, Fig. 8] experiment. Comparison between zero ampl. and LC ampl. See also Fig. 11
		0.862	From Noiray *et al.* [30, Fig. 9], experiment. Comparison between lin. unstable point LC and lin. stable LC (triggering)
-0.011 -0.055		1.001 1.012	From Gullaud *et al.* [31, table 3], estimated damping of perforated plates
	0.025		From Bothien *et al.* [32, Fig. 12], experiment
	0.125 -0.232	0.902	From Nicoud *et al.* [33, Fig. 13], Helmholtz solver with FTF from LES
		0.870 1.060 1.500 0.880	From Boudy *et al.* [34, Fig. 4, 5], experiment We treat this value as an outlier and discard it
	0.072		From Boudy *et al.* [35, Fig. 4, 7, mode 2], experiment
-0.021			From Boudy *et al.* [35, page 1126], experiment
		1.044 0.836	From Palies *et al.* [36, Fig. 8, bottom left], experiment From Palies *et al.* [36, Fig. 9, bottom right], experiment
	-0.046	0.872 0.956 0.920	From Salas [37, Fig. 6.13, page 178], Helmholtz solver with a FTF extracted from LES
-0.009			From Schwing *et al.* [38, at cold conditions], experiment
	0.023		From Bothien *et al.* [39, Fig. 8, without dampers], annular heavy duty gas turbine
-0.039			From Bothien *et al.* [39, Fig. 8, growth rate reduction with dampers]
	0.047	0.958 1.051	From Silva *et al.* [40, Fig. 6], Helmholtz solver/experiment, with flame, varying the time delay
-0.109	0.239	1.071	From Silva *et al.* [40, Fig. 8, 9, mode C08, flame A], Helmholtz solver/experiment. See also [36]
-0.014			From Wagner *et al.* [41, Fig. 13, 14], experiment
-0.061 -0.032 -0.011 -0.012			From Stadlmair *et al.* [42, Fig. 5], experiment very common value in this reference From Stadlmair *et al.* [42, Table 2]
	0.019		From Bothien *et al.* [43, Fig. 12, $\Delta T/T = 2\%$], annular industrial gas turbine
		0.96 1.05	From Bothien *et al.* [43, Fig. 12, $\Delta T/T = 4\%$]
-0.010			From Bothien *et al.* [43, Fig. 9, growth rate reduction due to dampers]
-0.062 -0.047 -0.067			From Mejia *et al.* [25, Table 3, NR], experiment From Mejia *et al.* [25, Table 4, NR] From Mejia *et al.* [25, Table 6, NR]
-0.050			From Ghirardo *et al.* [44]. Damping of the dominant frequency of the model. Reported by the authors, not in the paper
-0.026	0.011		From Boujo *et al.* [45, Fig. 6], experiment
	0.011		From Noiray & Denisov [46, condition c3], experiment

we introduced $\alpha = \bar{\alpha}/\mu$, and μ is the Euclidean norm of the   eigenmode, defined as

$$\mu = \int_\Omega |\chi(r,z)|^2 \cos(n\theta)^2 d\Omega \tag{11}$$

2.1. Flame model

We neglect the effect of the transverse acoustic field on the the fluctuating heat release rate q coming from the flame, as studied previously by [55], and assume that q depends only on the longitudinal acoustic field in the mean flow field direction. This is a good approximation in the linear regime if one assumes axisymmetric flames [61], but not as much in the nonlinear regime at high amplitudes of acoustic transverse velocity, as measured experimentally by [62, 63] for a swirl stabilized turbulent flame. We also do not study the general case of a discrete number of flames, each modelled in terms of a generic flame describing function as carried out by [44]. Instead, we assume that the number of burners is large enough that the flame model $q[p]$ is homogeneous in the azimuthal direction, and the nonlinearity consists of a fundamental cubic saturation. We then model q as a nonlinear, time-invariant operator of the acoustic axial fluctuating velocity u_{ax} at the flame inlet. The reasoning behind this is that an acoustic fluctuation of the longitudinal velocity at the burner induces a perturbation of the fuel/air mixture fraction [64, 65, 66, 67]. The local flow field perturbation can also be amplified by flow instabilities (see e.g. [68, 69, 70] for laminar flames) and/or modulates the swirl in swirling flames [71], and both mechanisms lead to perturbations of the flame response [72, 73]. For a review of these and other mechanisms, refer to [74, 75]. The resulting transfer function typically involves a set of time delays τ_k, of standard deviations γ_k^2, and interaction indices n_k, all real valued quantities:

$$\frac{\hat{q}(\omega)}{\hat{u}_{ax}(\omega)} = \sum_k \pm n_k e^{-i\omega\tau_k} e^{-\gamma_k^2 \omega^2} \tag{12}$$

The structure of this transfer function holds also for turbulent flames, see e.g. [76, 73, 71, 56]. The fluctuating axial velocity u_{ax} can be expressed as a linear transfer function of the pressure p in the annular chamber, as long as only one mode, or two degenerate modes, oscillate, as discussed in detail in [44]. In particular one can write

$$\frac{\hat{u}_{ax}(\omega)}{\hat{p}(\omega)} = A^n(\omega) = \beta^*(\omega) e^{i\xi(\omega)} \tag{13}$$

where $A^n(\omega)$ is the admittance of the whole part of the combustor upstream of the section where u_{ax} is measured, calculated for the n-th azimuthal instability. This admittance depends on the upstream geometry and boundary conditions and on the burner transfer matrix. From (12) and (13) it follows that

$$\frac{\hat{q}(\omega)}{\hat{p}(\omega)} = \beta^*(\omega) e^{i\xi(\omega)} \sum_{k=1}^{N_k} \pm n_k e^{-i\omega\tau_k} e^{-\gamma_k^2 \omega^2} \tag{14}$$

Despite the quite complicated expression of (14), this transfer function typically exhibits a gain with a certain number of bumps[4] as function of the frequency, and a phase that decreases with frequency[5]. This holds both in the linear and nonlinear regime, see e.g. [30] for a matrix burner and [77] for a swirl burner. This means that in the neighbourhood of the acous-

[4]sequence of local maxima and minima alternating along the frequency axis
[5]this is the case of most cases of interest. The flame phase can sometimes increase, usually in small ranges of frequencies in which the gain is low
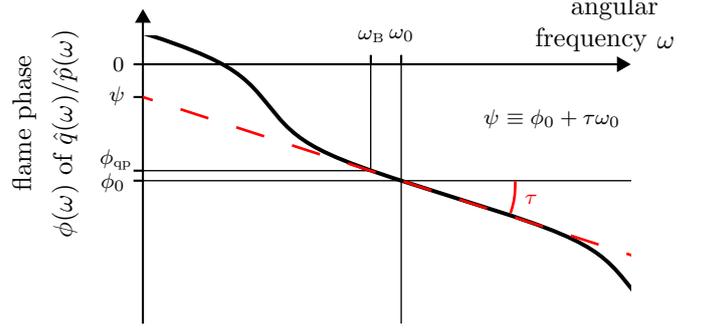
Figure 1: Flame phase, i.e. phase of $\hat{q}(\omega)/\hat{p}(\omega)$. In the vicinity of the frequency ω_0 of the acoustic mode we approximate the phase response $\phi(\omega)$ (black line) with a straight line (red dashed line). The value of the phase at ω_0 is $\phi_0 \equiv \phi(\omega_0)$. We define the equivalent time delay τ as minus the local slope of the phase in ω_0. The results are obtained first for the case of $\psi = 0$, for which the model becomes $q = p(t-\tau)$, and generalized later. The frequency of the thermoacoustic system can shift from ω_0 to the frequency ω_B such that the phase ϕ_{qp} between the fluctuating heat release rate q and the acoustic pressure p is more favourable

tic frequency ω_0 of the azimuthal mode of interest (14) can be simplified to:

$$\frac{\hat{q}(\omega)}{\hat{p}(\omega)} = \beta e^{i\phi(\omega)} \tag{15a}$$

$$\phi(\omega) = \phi_0 - \tau(\omega - \omega_0) \quad \text{with } \phi_0 \in [-\pi, \pi] \tag{15b}$$

where τ is an equivalent time delay and describes the local slope of the flame phase close to ω_0, i.e. $\tau \equiv -\partial\phi(\omega = \omega_0)/\partial\omega$ and ϕ_0 is the value of the flame phase for $\omega = \omega_0$. A sketch of the flame phase $\phi(\omega)$ and of the linear approximation in the vicinity of ω_0 is presented in Fig. 1. In (15) we also choose a constant real valued gain β with frequency because in the general case there is no established trend, i.e. the gain can either grow or decay with frequency due to the bumps mentioned earlier. We introduce the quantity $\psi \equiv \phi_0 + \tau\omega_0$ and observe that if we set it to zero the red dashed line in Fig. 1 passes through the origin. This means that the exponential in (15) becomes $\exp(-i\omega\tau)$ and we can write in the time domain that $q = \beta p(t - \tau)$. In the following we first simplify the discussion by setting $\psi = 0$ and generalize the results later for $\psi \neq 0$. This simplification allows us to interpret $-\tau\omega$ as the phase between $\hat{q}$ and $\hat{p}$.

In the time domain and in the nonlinear regime, we can write

$$q(t) = \beta p(t - \tau) - \kappa p(t - \tau)^3 \tag{16}$$

In (16) κ is a positive valued constant describing how fast with amplitude the flame response saturates. Applying the definition (3) on $q[p]$ from (16) we obtain the describing function Q:

$$Q(A, \omega) = \left(\beta - \frac{3}{4}\kappa A^2\right) e^{-i\omega\tau} \tag{17}$$

where the first factor is the gain $G(A)$ of the describing function. We are making two key assumptions in (16-17). The first regards the chosen cubic saturation, which is fundamental and simple as discussed by [48], and features a monotonic decrease

of the gain $G(A)$ with the amplitude A, which is usually the case. The effect of a non monotonic decrease of the flame gain with the amplitude [78] on the system's stability is well understood in the literature, see e.g. [19, 79] for axial instabilities and [44, 80] for azimuthal instabilities.

The second regards the delay τ that is assumed to be constant in the linear and nonlinear regime, so that the phase response ϕ does not depend on the amplitude A. The phase dependence with amplitude is usually weak, see [81; 82; 56, Fig. 12; 71, in the conclusions], and is a less common mechanism of saturation to limit cycles, with a few notable exceptions, see e.g. the matrix burner at EM2C [13, Fig. 11 above 900 Hz]. Saturation of a thermoacoustic system to a limit cycle is usually governed by the drop of the flame gain $|Q(A, \omega)|$ with amplitude. We also constrain the phase to not depend on amplitude to investigate specifically the effect of the slope τ of the phase response as introduced in (15). This will also allow us to compare the model with a successful low order model that exists already [83, 84], which has been used to identify growth rates in real system.

2.2. Model equations

By substituting (16) into (9) we obtain

$$\eta_1''(t) + \omega_0^2 \eta_1(t) = f(\eta_1'(t), \eta_1'(t-\tau), \eta_2'(t-\tau)) \quad (18a)$$
$$\eta_2''(t) + \omega_0^2 \eta_2(t) = f(\eta_2'(t), \eta_2'(t-\tau), \eta_1'(t-\tau)) \quad (18b)$$

where the function f is defined as:

$$f(a, a_\tau, b_\tau) \equiv a_\tau \left[\beta - \frac{3}{4}\kappa \left(a_\tau^2 + b_\tau^2 \right) \right] - \alpha a \quad (19)$$

where we denote with a subscript τ a delayed quantity, e.g. $a_\tau(t) = a(t - \tau)$. An example of a time domain simulation of the oscillators (18) is presented in Fig. 2, where in a) the continuous thin lines are the fast oscillating signals $\eta_1(t)$ and $\eta_2(t)$, and the thick lines are their slowly varying amplitudes of oscillation $A_1(t)$ and $A_2(t)$. In Fig. 2.b we present the instantaneous frequency of oscillation of the same simulation with a black line. To link this study with the existing literature, we remark that one can take the time derivative of (18) and obtain:

$$\zeta_1''(t) + \omega_0^2 \zeta_1(t) = \frac{\partial}{\partial t} f(\zeta_1(t), \zeta_1(t-\tau), \zeta_2(t-\tau)) \quad (20a)$$
$$\zeta_2''(t) + \omega_0^2 \zeta_2(t) = \frac{\partial}{\partial t} f(\zeta_2(t), \zeta_2(t-\tau), \zeta_1(t-\tau)) \quad (20b)$$

where the function $\zeta_j(t) \equiv \eta_j'(t)$ was introduced. By setting τ to zero in (20) one recovers the equations discussed in [48]. One disadvantage of the second formulation (20) of the problem is the additional time-derivative of the function f that includes the heat release rate and leads to the study of the problem with mixed terms $\zeta_j^k(t)\zeta_j'(t)$ in the equations.

We mention that any stochastic contribution $q_s(t)$ to the heat release rate appears on the right hand sides of (18) after spatial averaging, and hence should appear in (20) as a time derivative, and not outside of the time derivative as presented in [85]. We stick to the formulation in terms of equations (18) in the following.

2.3. The case of an axial mode

When carrying out the projection of the equations (7) on a single mode η_1 one obtains

$$\eta_1''(t) + \omega_0^2 \eta_1(t) = f(\eta_1'(t), \eta_1'(t-\tau)),$$
$$\text{with} \quad f(a, a_\tau) = a_\tau(\beta - \kappa a_\tau^2) - \alpha a \quad (21)$$

Note that the definition of μ for an axial mode stays the same, but since the mode does not depend on the azimuthal component (11) becomes

$$\mu = \int_\Omega |\chi(r, z)|^2 d\Omega \quad (22)$$

Results of §3 and §4 apply for axial modes too. We will discuss in particular the case of an axial mode later in §4.5 and in §5.

2.4. Range of the parameters $\{\alpha, \beta, \tau\omega_0\}$

In this manuscript all the analytical expressions are valid for $\{\beta, \alpha\} \in \mathcal{R}^{+2}$ and $\tau \in \mathcal{R}$ unless otherwise indicated. It is however important to estimate the range of typical values of these parameters in thermoacoustics.

Based on the first column of Table 1 we consider as typical a thermoacoustic system with a level of acoustic damping such that the negative nondimensional growth rate σ/ω_0 equals -0.04 when the flame response is shut off. We then consider the case of a zero time delay τ, for which the growth rate of the system is $(\beta - \alpha)/2$ as discussed in [48]. When the flame response is shut off, i.e. $\beta = 0$, we obtain the value of the nondimensional acoustic damping coefficient $\alpha/\omega_0 = 0.08$, which we keep fixed in the following. We will reconsider the role of α/ω_0 in §3.4.

Based on the relative values of the first two columns of Table 1, we consider a strongly unstable system to have a positive, linear nondimensional growth rate σ/ω equal to 0.08 when both damping and flame act on the acoustic field. This leads to a ratio $\beta/\omega_0 = 0.12$, and a ratio $\beta/\alpha = 3$. We then decide to study in the following the system for $\beta/\alpha \in [1, 3]$, where values of β smaller than 1 will be found to be trivially stable in the next section.

For estimating the range for $\tau\omega_0$, we consider an example of a thermoacoustic mode at $f = 300$ Hz, subject to a convective time delay of $\tau = 5$ ms. For example we will later discuss one thermoacoustic mode at $f_0 \approx 1000$ Hz of [34], for which $\tau\omega_0 = 3\pi$ based on their Fig. 7. This leads to a product of $\tau\omega_0 \approx 3\pi$. Note moreover that the superposition of different time delays often leads to a steeper flame phase in certain frequency ranges. In these ranges, the equivalent time delay $\tau\omega_0$ discussed just after (15) would be even larger. Accounting for longer time delays and larger frequencies of oscillation, in the following we study the system for $\tau\omega_0 \in [0, 8\pi]$. To summarize, we investigate:

$$\begin{cases} \beta/\alpha \in [1, 3] \\ \tau\omega_0 \in [0, 8\pi] \end{cases} \quad \text{for} \quad \alpha/\omega_0 = 0.08 \quad (23)$$

and we will reconsider the role of the level of acoustic damping α/ω_0 in §3.4.
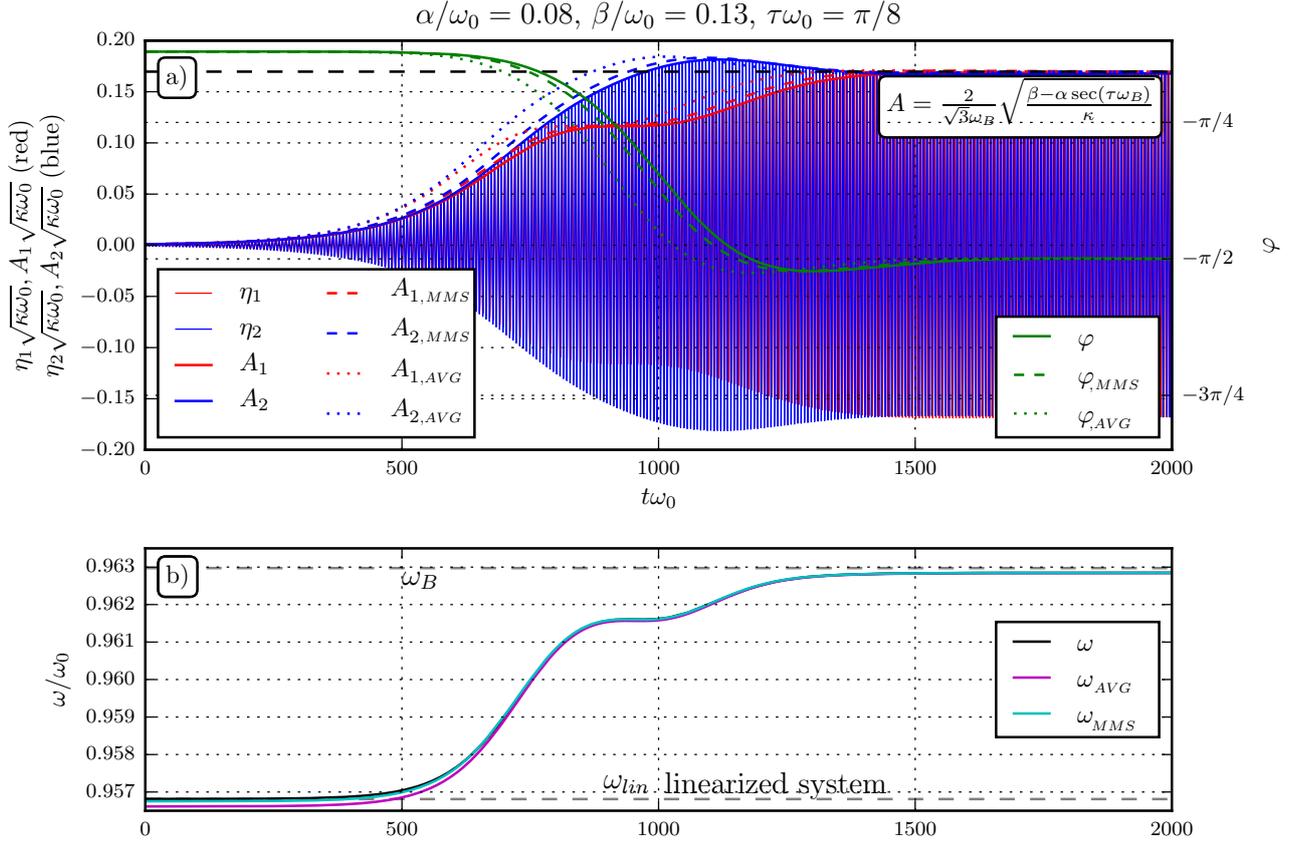
Figure 2: a) Example of time domain simulation of the two azimuthal modes η_1 and η_2 of an annular combustor chamber. The fast oscillating pressure values $\eta_j(t)$ are obtained by integrating the original system of equations (18) (continuous lines), while the slowly varying amplitudes of oscillation A_j are obtained with the method of multiple scales (MMS, dashed lines) and alternatively with the averaging method (AVG, dotted lines). In this case we choose $\tau\omega_0 = \pi/8 \neq 0$ and this leads to a non-trivial response: the two amplitudes A_j undergo a non-monotonic transient where A_1 overshoots the final amplitude and A_2 grows more slowly than A_1. b) Dependence of the frequency of oscillation on time: ω is the calculated instantaneous frequency of oscillation extracted from the modes η_j, while ω_{AVG} and ω_{MMS} are the predicted instantaneous frequencies using the method of multiple scales (MMS) and the averaging method (AVG). In a) and b) both nonlinear methods have both good accuracy in predicting the slowly varying amplitudes and the instantaneous frequency

3. Linear analysis

We first tackle in §3.1 the case where in Fig. 1 the response ψ at zero frequency is zero, and then generalize the results in §3.2 to $\psi \neq 0$.

3.1. Simplified case with $\psi \equiv \phi_0 + \tau\omega_0 = 0$

In this section we study the boundary of linear stability of (18). We proceed by retaining only the linear terms in (18a) and (18b), and obtain:

$$\eta_j''(t) + \alpha\eta_j'(t) - \beta\eta_j'(t-\tau) + \omega_0^2\eta_j(t) = 0 \qquad j = 1, 2 \quad (24)$$

We observe that in the linear regime the equations for the azimuthal and axial modes match, so that the analysis of (24) carried out in this section applies to both cases. We substitute $\eta_1(t) = e^{(\sigma+i\omega)t}$ into (24) where σ is the growth rate and ω the real valued angular frequency of oscillation, and obtain the characteristic equation. We then split the equation into real and

imaginary parts and after some manipulation obtain:

$$\frac{\beta\cos(\tau\omega)e^{-\sigma\tau} - \alpha}{2} = \sigma\left[1 + \frac{\beta\tau}{2}\text{sinc}(\tau\omega)e^{-\sigma\tau}\right] \quad (25a)$$

$$\omega^2 - \omega_0^2 + \beta\omega\sin(\tau\omega)e^{-\sigma\tau} = \sigma^2 + \alpha\sigma - \beta\sigma\cos(\tau\omega)e^{-\sigma\tau} \quad (25b)$$

We study for which parameters $\{\alpha, \beta, \tau\} \in \mathbb{R}^{+^3}$ the system is neutrally stable, i.e. there exist real-valued solutions ω_B of the system of equations (25) when setting the growth rate σ to zero:

$$\beta\cos(\tau\omega_B) - \alpha = 0 \quad (26a)$$

$$\omega_B^2 - \omega_0^2 + \beta\omega_B\sin(\tau\omega_B) = 0 \quad (26b)$$

In (26), we call ω_B the thermoacoustic frequency of the system, as opposed to ω_0 that is the acoustic frequency, where the subscript refers to the fact that it is calculated on the boundary of stability. We observe that the left hand side of (26a) is the difference between the real part of the transfer function $Q(A = 0, \omega_B)$ minus the gain α of the acoustic losses, both projected on the mode shape as discussed just after (9). This conveys the same information as the Rayleigh criterion (6), but

with an equal sign since we are looking for the boundary of neutral stability.

Equation (26b) is the key ingredient that was missing in the introduction to quantify how a thermoacoustic eigenmode can shift its frequency of oscillation due to the flame response. It resembles (21) of [23] as discussed in the introduction. In particular the last term on the left hand side is $\omega_B \text{Im}[Q(A = 0, \omega)]$, i.e. ω_B times the imaginary part of the describing function calculated at zero amplitude. This terms act as a perturbation in the equation, in the way that ω_B deviates from ω_0 as this term increases. In particular this frequency shift from ω_0 to ω_B is zero if the phase is zero or a multiple of 2π, as expected. We carry out with rigour the analysis of the implicit dispersion relation $\omega_B = \omega_B(\beta/\alpha, \tau\omega_0)$ in the appendix §A, but we mention here that the frequency ω_B at the boundary of stability is calculated as the root of

$$h(\tau, \omega_B) \equiv \omega_B^2 - \omega_0^2 + \alpha\omega_B \tan(\tau\omega_B) = 0 \qquad (27)$$

We present in Fig. 3.a the stability map of the system, where the ranges of the horizontal and vertical axes are representative of a class of thermoacoustic systems as discussed in §2.4. The boundary of stability is reported with a coloured line as a function of the nondimensional slope $\tau\omega_0$ introduced in (15), where ω_0 is the natural acoustic frequency of the system and τ is the slope of the flame phase close to ω_0. Above this boundary of stability the system is linearly unstable and the region is coloured with grey. The colour of the boundary is the linear frequency of oscillation ω_B/ω_0 of the system and the respective colourmap is reported on the right.

Where $\tau\omega_0$ is a multiple of 2π we have that $\omega = \omega_0$ and q is exactly in phase with p, and the required ratio β/α to render the system neutrally stable equals unity and is minimum, as expected from the Rayleigh criterion. As the value of $\tau\omega_0$ gets farther away from a multiple of 2π, the strength of the flame response required to de-stabilize the system increases, and the curve β/α takes the form of a trough with the minimum at each multiple of 2π.

Moreover, the width of the troughs increases with the multiples of 2π, so that the boundary of stability approaches the horizontal asymptote $\beta/\alpha = 1$ as $\tau\omega_0 \to \infty$. This means that for a given system with a fixed ratio of β/α, flames governed by large time delays, i.e. equivalently flames with a steep phase in the vicinity of the acoustic frequency ω_0, are more likely to be unstable than flames governed by smaller time delays, and the overall system's stability is less affected by the flame phase close to the frequency of oscillation. In other words, for a fixed flame gain, a flame with a steeper phase is more likely to excite an acoustic mode, because the troughs in Fig. 3.a are wider. These results compare well with [86, Fig. 6,7], who plot one over the expected mean value of the amplitude of oscillation, for a a similar[6] set of linear equations forced with gaussian additive white noise.

---

[6]Crawford *et al.* [86] study only axial modes, for which case it is more straightforward to study q as function of the acoustic velocity instead of the acoustic pressure, as [86] do. This leads to a different delay definition. Their Fig. 6 and 7 should be compared for $\varepsilon_v < 0$, where $-\varepsilon_v$ plays the same role of β of this manuscript

Figure 3.b presents the same information as Fig. 3.a but swapping the vertical axis with the colourmap. In Fig. 3.b, where $\tau\omega_0$ is a multiple of 2π, the frequency ω_B matches the natural frequency of oscillation ω_0. For values of the time delay $\tau\omega_0 < \pi/2$ the linear frequency of oscillation ω_B is smaller than the natural frequency of oscillation ω_0. We observe that for values of $\beta/\alpha < 3$ we can see a linear frequency shift of up to about 10% even for small values of $\tau\omega_0$. This is in line with the experimental findings reviewed in the introduction. This will be confirmed in §4 also in the nonlinear regime, and shows how assuming that the frequency of oscillation of the system matches the natural frequency of oscillation ω_0 is a rough approximation.

Fig. 3 generalizes the linear results observed in [26] for a specific combustor and flame, where a parametric study of the linear growth rate as function of the delay is presented in their Fig. 7, reproduced here in Fig. 4. In particular the contour lines of the growth rate in that figure follow the same pattern presented in Fig. 3. This shows how the assumption of studying one acoustic mode leads to results that are in good agreement with numerical analyses where all modes are considered.

In the same Fig. 3.a and 3.b we present with black lines the result obtained neglecting the part of heat release rate out of phase with the pressure, as assumed in [47, 48], so that one can compare the results with and without this assumption. The derivation is in §A.1. In Fig. 3.a we observe that the black troughs are exactly the same and simply shifted by 2π on the horizontal axis $\tau\omega_0$, so that the error on the boundary of instability increases for larger values of $\tau\omega_0$. As expected, in Fig. 3.b we show how the predicted frequency of oscillation matches ω_0 at all linearly unstable conditions.

3.2. Generalization to $\psi \equiv \phi_0 + \tau\omega_0 \neq 0$

In Fig. 5 we present the results for the more general flame response presented in Fig. 1. In particular the vertical and horizontal axis of Fig. 5 are the flame phase and the nondimensional flame phase slope of Fig. 1. We refer the reader to §A.2 for how these results are obtained from the results of Fig. 3. We observe that for a fixed ratio β/α depicted by respective pairs of red lines, the system is unstable and pulsates if the point $(\tau\omega_0, \phi_0)$ is between the two red straight lines, and does not pulsate otherwise. The frequency of oscillation ω_B at the boundary of stability is presented with the colourbar. We will prove in §4.2 that the frequency ω_B matches the frequency at the limit cycle, so that the colourbar of Fig. 5.a applies also to the limit cycle solutions. For a constant nondimensional flame phase slope $\tau\omega_0$, the most favourable value of the phase ϕ_0 to make the system pulsate is zero, which is the case where the thermoacoustic frequency ω_B matches the acoustic frequency ω_0. If within a period of oscillation the fluctuating heat release rate comes later in time than the acoustic pressure, ϕ_0 is negative and the thermoacoustic frequency ω_B is be lower than the acoustic frequency ω_0, i.e. in the Fig. $\omega_B/\omega_0 < 1$. If instead the fluctuating heat release rate occurs before the acoustic pressure, ϕ_0 is positive and ω_B is larger than ω_0. For the limit case of $\beta/\alpha = 1$ the unstable region shrinks to the line $\phi_0 = 0$,
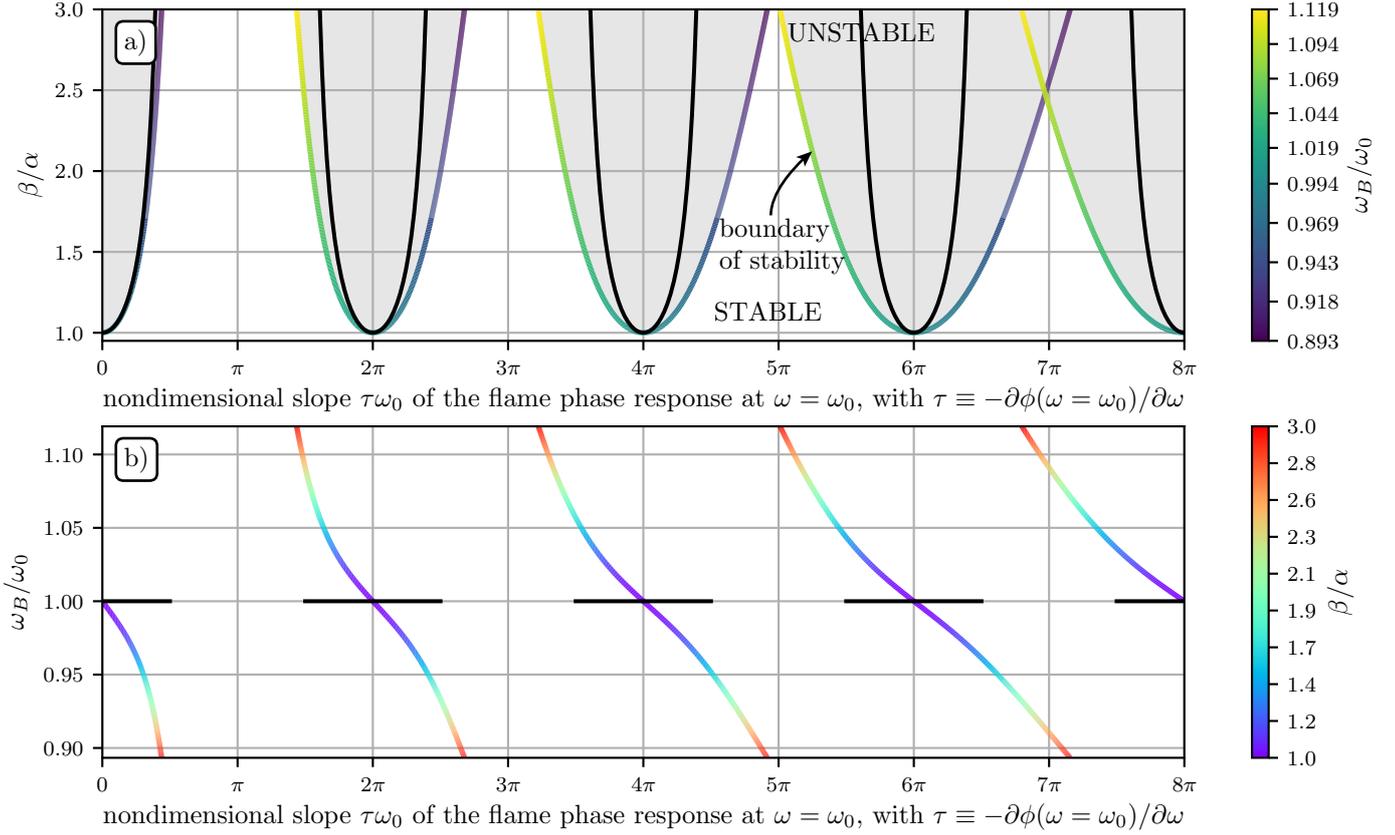
Figure 3: Results for the simplified case with $\psi = 0$ in Fig. 1. Linear stability analysis of axial and azimuthal thermoacoustic modes characterized by a natural frequency of oscillation ω_0, and a flame response $q[p] = \beta p(t - \tau)$. a) Boundary of neutral stability as function of the local slope $\tau\omega_0$ of the flame phase. The coloured line is the ratio of the linear driving β over the acoustic damping α to make the system neutrally stable. The linearly unstable region is filled in grey. b) The coloured line is the frequency of neutral stability ω_B/ω_0 on the boundary described in a). In both frames the black line is the simpler solution obtained neglecting the part of the heat release rate q not in phase with the pressure p as assumed in [47, 48]
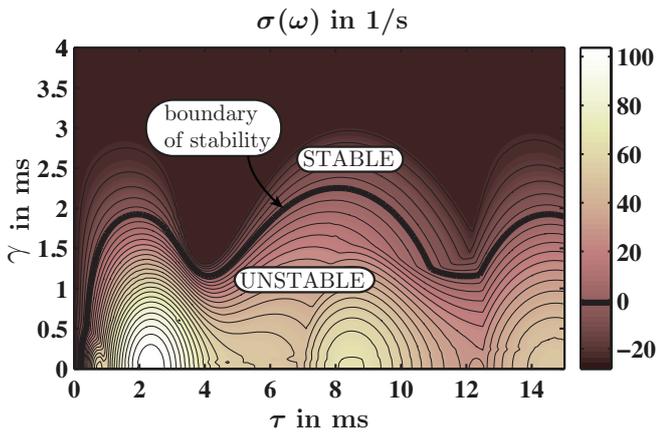
Figure 4: Growth rate of the mode at frequency $\omega_0/2\pi \approx 100$ Hz as a function of the convective mean delay τ and of the standard deviation γ of the time delays for the specific combustor studied by [26]. This result was obtained with a stability analysis that accounts for all modes and by approximating the time delay τ with a Pade approximation. Large values of standard deviation γ lead to small values of the ratio β/α in Fig. 3, so that the two vertical axes here and in Fig. 3 are reversed when comparing them. The border of stability presented with the thick line follows the same trend of the border of stability of Fig. 3. This showcases the validity of projecting the equations on one thermoacoustic mode only as applied in this manuscript. Readapted from [26].

which requires that the phase between pressure and heat release rate is exactly zero.

We now discuss the first scenario introduced in the introduction, where the flame phase ϕ_0 is $-\pi$. The term on the left hand side in the Rayleigh criterion (6) is negative at ω_0 and one is then tempted to conclude that the acoustic mode will be stable and pulsations will not be observed. In Fig. 5.a we then focus on the line $\phi_0 = -\pi$, and we want to determine whether the system pulsates or not. We observe that for $\tau\omega_0 \lesssim 5\pi$ the point is always in the white region and the system will not pulsate. However for larger values of $\tau\omega_0$ the system will pulsate if it falls between the two red lines for a given ratio of β/α. We can then conclude that the system will be unstable if the slope of the phase response is sufficiently steep and the flame gain is sufficiently steep. This can be intuitively understood by the fact that if the flame has a steep phase at the resonance frequency ω_0, even a little shift of the frequency from ω_0 can lead to a variation of the phase between q and p sufficient to obtain a phase ϕ_{qp} between heat release rate and acoustic pressure that is favourable to pulsations. This can be confirmed by looking at Fig. 5.b, where we present the phase ϕ_{qp}. One can observe that along horizontal lines larger values of $\tau\omega_0$ lead to a value of the phase ϕ_{qp} closer to zero, i.e. more favourable for pulsations.

We can similarly also address the second scenario, which
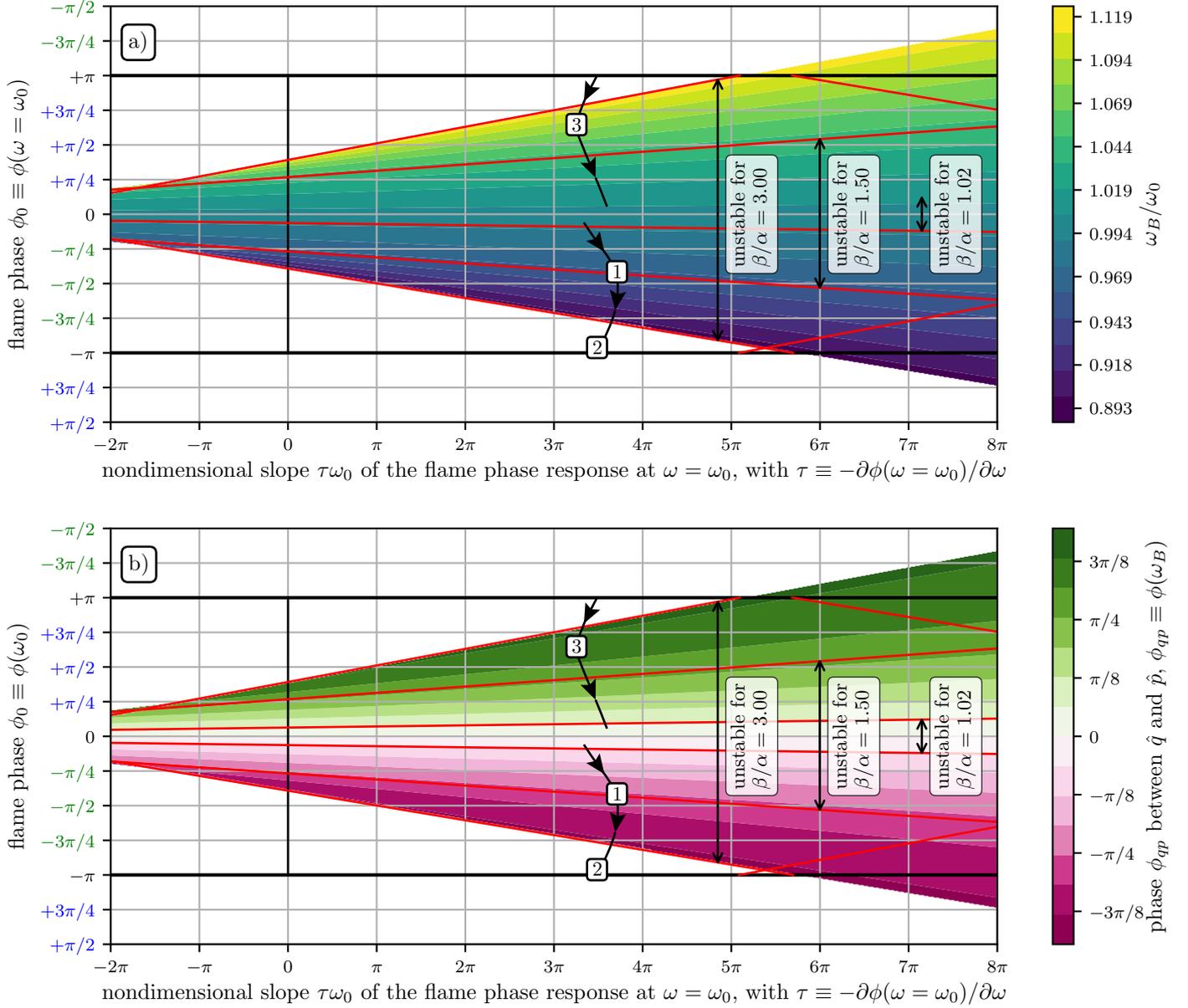
Figure 5: Stability boundary of an acoustic mode at frequency ω_0 coupled to a flame with nondimensional gain β and phase $\phi(\omega) = \phi_0 - \tau(\omega - \omega_0)$ as presented in Fig. 1. In both figures the vertical axis is the phase $\phi_0 = \phi(\omega = \omega_0)$ between heat release rate q and the acoustic pressure at the flame location p, calculated at $\omega = \omega_0$. The horizontal axis is the nondimensional slope of the flame phase $\tau\omega_0$. The boundary of stability depends parametrically on the ratio of the flame linear driving β over the level of acoustic damping α. For a fixed ratio β/α, the system is unstable between the two red lines linked by the black arrow.

In a) we present the frequency of oscillation ω_B in terms of the ratio ω_B/ω_0 on the colourbar on the right. ω_B is both the frequency of oscillation on the boundary of instability as introduced in §3 and also the frequency of oscillation of the limit cycle solution as proved in §4. The domain in the vertical axis is periodic in $[-\pi, \pi]$ and lies between the two horizontal thick black lines. It is extended beyond its periodic boundaries to plot both frequency shifts in the two regions where the two colours would overlap. Note that if the slope of the phase $\tau\omega_0$ is larger than approximately 5π, for a value of $\beta/\alpha = 3$: a) the system pulsates regardless of the phase ϕ_0; b) the system admits two limit cycle solutions at two different frequencies, one larger and one smaller than ω_0, in the two regions at the top and at the bottom where the red lines cross. The range of frequency shifts from ω_0 is in line with the literature discussed in the introduction.

In b) we present the phase ϕ_{qp} between heat release rate q and pressure p. This value is valid both on the boundary of stability and in the nonlinear regime, and is consistent with experimentally determined values [87, 88]. The black arrow is the interpretation of an experiment [34], detailed in §3.3

considers a thermoacoustic system that is already pulsating, to whose flame phase π is added. In Fig. 5.a this corresponds to moving the point vertically by π. If the point moves to the white region the addition of π makes the system stable. Similarly to the previous result, this is more likely to happen on the left part of the figure, i.e. with flames with non steep phase responses, and secondarily if the ratio β/α is small.

One observes how for quite a small value of $\beta/\alpha = 1.5$ and for not steep flame phases $\tau\omega_0 \approx 0$ the range of the phase ϕ_0 at which the system is unstable is already quite broad, approx-

11

imately $[-\pi/4, \pi/4]$. If $\tau\omega_0$ is increased, the unstable range for ϕ_0 leading to pulsations becomes larger, and is one of the novel results of this paper. The same applies if the ratio β/α of the strengths of flame response and acoustic damping increases, consistent with the literature that higher flame gains lead to larger unstable regions. This allows us to partially discuss the third scenario. We find that the actual value of the phase ϕ of the flame transfer function is not a feature strongly linked with the risk of an unstable combustor if the slope of the phase is steep, and secondarily if the flame gain is very large. This means that if the flame phase is sufficiently steep and/or the flame strength β sufficiently strong, the system will pulsate regardless of the flame phase $\phi(\omega)$. Moreover when comparing two flames with the same gain, the one with steepest phase has a higher pulsation risk. However, one should not jump to the more general but hasty conclusion that shorter values of τ lead to fewer pulsations. For example longer convective time delays from the injection point lead to better mixing which reduces in turn the amplitude of equivalence ratio fluctuations at the flame, and longer flames have a larger standard deviation γ in (14). Both factors usually lead to a smaller equivalent gain β in (15), as discussed for one particular system in Fig. 4.

We observe how there is a region on the right of Fig. 5.a where there exist two different frequencies of oscillation. In particular the yellow triangle above the line $\phi_0 = \pi$ actually overlaps the indigo blue triangle below the line $\phi_0 = -\pi$. In the nonlinear regime, either one of the two could take over. The numerical simulations suggest that, for the simple nonlinear saturation model considered in this manuscript, the limit cycle solution with the higher linear growth rate prevails over the other. This would mean that in the experiments only the strongest mode of the two would be observed, making validation difficult.

We present in Fig. 5.b the same data, but plot in colour the phase ϕ_{qp} between the heat release rate q and acoustic pressure p. The critical value of $|\phi_{qp}|$ on the boundary of stability is smaller than $\pi/2$ because of the acoustic damping, as discussed by [88], and agrees well with their experimental values. [88] concludes that the phase ϕ_{qp} *[. . .] may be used to quantify the state of the combustor within a dynamic mode*. Consistently, we observe in Fig. 5.b that ϕ_{qp} is a good metric for how close to the boundary of neutral stability the mode is. The critical values of $|\phi_{qp}|$ slightly larger than $3\pi/8$ on the boundary of stability for $\beta/\alpha = 3$ compare well with the maximum experimental values measured by [88, Fig. 6]. The range covered by ϕ_{qp} depends on the ratio β/α. For example the range of ϕ_{qp} found by [87, Fig. 8] to be approximately $[-\pi/4 , \pi/4]$ corresponds in Fig. 5.b approximately to $\beta/\alpha \approx 2$.

3.3. Interpretation of one thermoacoustic transition observed by Boudy et al. [34]

We conclude this section with the interpretation of one experiment using the results of Fig. 5. Boudy *et al.* [34, Fig. 4] characterize a combustor that during a controlled parametric reduction of the feeding manifold L_1 transitions through three states: *1)* the pulsation frequency decreases from the acoustic frequency ω_0 of the second mode, with a decreasing ratio

ω_B/ω_0; *2)* the combustor stays quiet for a small interval of ΔL_1; *3)* the combustor pulsates again, but on the other side of ω_0, with $\omega_B > \omega_0$. In the two pusating states the amplitude $u'_{\text{rms}}/U_{\text{bulk}}$ of the limit cycles stays in the range $[0.2 , 0.3]$ [34, Fig. 8], where the phase slope is quite constant [34, Fig. 7]. With reference to Fig. 5, one can interpret the transition between the first two states as a point in the figure moving down from $\phi_0 = 0$, with a ratio ω_L/ω_0 dropping. This is qualitatively presented in the Figure with a black arrow passing through the three states 1,2,3. Due to the change of the frequency ω_0 which now approaches $900\,\text{Hz}$, the gain of the flame reduces [34, Fig. 7]. As a result, the unstable region shrinks towards the line $\phi_0 = 0$, the point exits the unstable region from the bottom and the combustor becomes stable. Due to the reduction of L_1, we have a change of ω_0 and of the phase ϕ_0, and the point continues going down and reenters the domain from the top due to the periodicity. When it touches the top boundary of stability, the system pulsates at a frequency now larger than ω_0. Further reduction of L_1 leads to a decrease of ϕ_0 towards 0 so that the frequency ω_B approaches ω_0. This subsection showed how the proposed model captures the transition between different thermoacoustic states, and amplitude and frequency variations that are typical of thermoacoustic systems.

3.4. Sensitivity to the level of acoustic damping

As discussed at the end of §2.4, the plots presented so far are for a value of $\alpha/\omega_0 = 0.08$, which we chose as representative of a class of thermoacoustic systems. In general this value depends on very many factors, e.g. the compactness of the combustion system, the flow path, the installation of acoustic dampers, the acoustic dissipation at the combustor boundaries, the Mach number of the flow, etc.. We conclude this section by discussing the sensitivity with respect to this value. We present in Fig. 6 the same results of Fig. 5 but for $\alpha/\omega_0 = 0.04$. Because we fix the ratio β/α to the same range $[0, 3]$, we find that smaller values of α and hence β lead to smaller frequency shifts of ω from ω_0 for a fixed value of $\tau\omega_0$ in Fig. 3.b. Physically, this has the simple interpretation that if the acoustics are little damped and little amplified, the acoustic frequency is little affected by them. Conversely, the smaller frequency shift leads to a smaller change in the phase ϕ, resulting in a weaker dependence of the boundary of stability on the slope of the phase.

4. Nonlinear analysis

The main objective of this section is to extend the validity of the results obtained on the boundary of stability in the linear regime to the nonlinear regime. In particular this will allow us to interpret ω_B and ϕ_{qp} as the limit cycle frequency and the limit cycle flame phase. To this aim we apply two nonlinear methods to predict analytically the amplitudes and frequencies of oscillation. As compared to previous work on the topic, the major technical novelty of this section is in the fact that we explicitly calculate how the instantaneous frequency of oscillation varies as a function of the amplitudes of oscillations, instead of fixing it to a constant value, as presented for example in Fig.
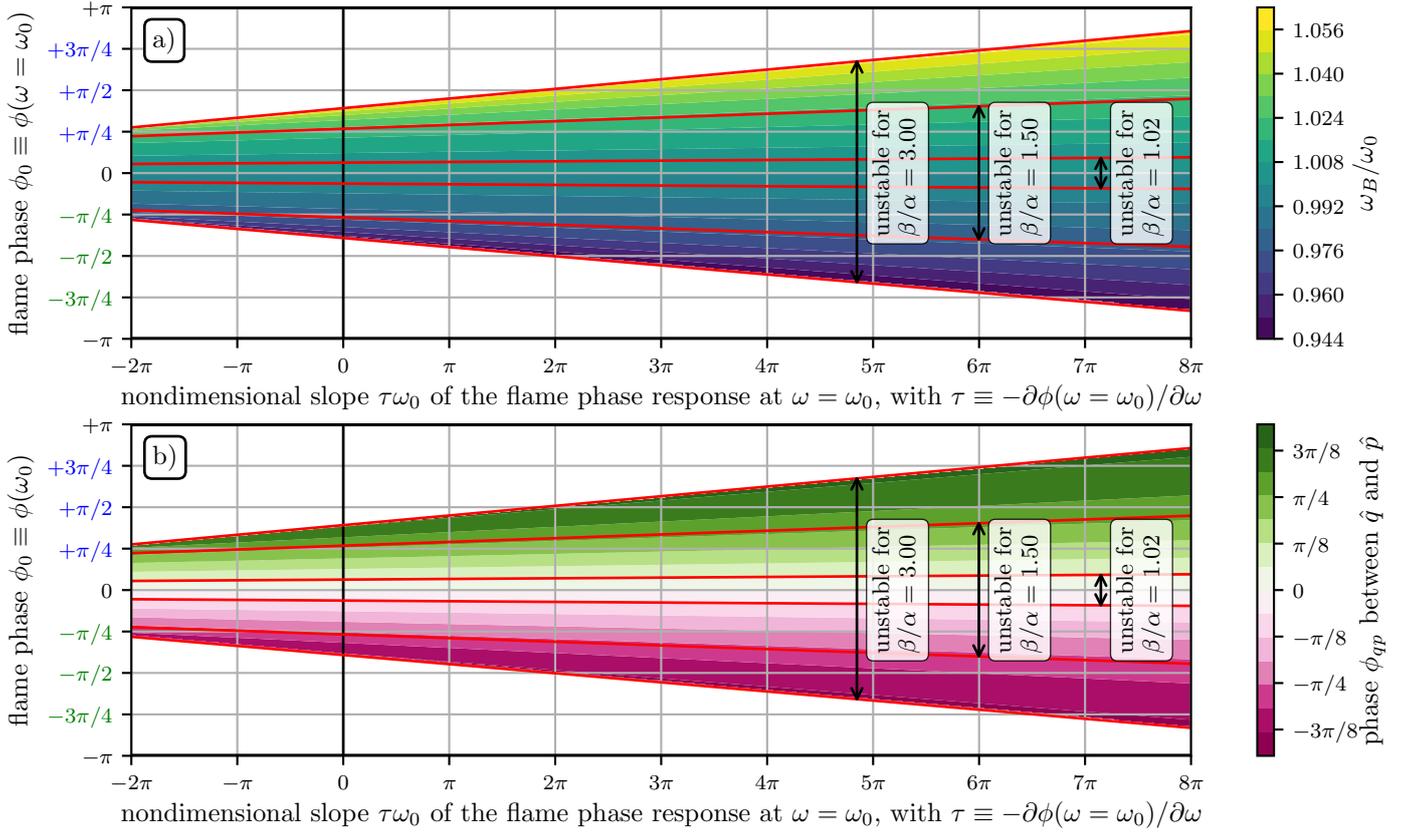
Figure 6: Same as Fig. 5, but for a level of acoustic damping $\alpha/\omega_0 = 0.04$ instead of 0.08. Since the investigated range of β/α is the same as Fig. 5, this case presents smaller forcing terms f on the right hand side of (18), the acoustic field is less perturbed and the thermoacoustic frequency ω_B in a) is closer to ω_0 than in Fig. 5.

2.b. The section is structured so that a reader mostly interested in the results can directly start reading at §4.6. In §4.1 we apply the method of averaging and in §4.2 we discuss the choice of the frequency of oscillation. In §4.3 we apply the method of multiple scales and in §4.4 we validate both methods numerically.

4.1. Method of averaging

In this section we apply first order averaging to the model, as defined and discussed in [89]. We rewrite (18) as a first order system $(x_j, y_j) \equiv (\eta_j, \eta_j')$:

$$x_j'(t) = y_j(t) \tag{28a}$$
$$y_j'(t) = -\omega_0^2 x_j(t) + f_j \tag{28b}$$

where $f_1 = f(y_1(t), y_1(t-\tau), y_2(t-\tau))$ and $f_2 = f(y_2(t), y_2(t-\tau), y_1(t-\tau))$. We introduce the change of variables $(x_j, y_j) \rightarrow (A_j, \varphi_j)$:

$$\begin{cases} 2x_j(t) = A_j(t)e^{i(\omega t + \varphi_j(t))} + \text{c.c.} \\ 2y_j(t) = i\omega A_j(t)e^{i(\omega t + \varphi_j(t))} + \text{c.c.} \end{cases} \tag{29}$$

where c.c. denotes the complex conjugate of the expression to its left. Note that we do not constrain the oscillation frequency ω in (29) to match the acoustic frequency ω_0. The application

of the method of averaging is standard (see appendix §B) and assumes that the delay is small compared to the slowly varying timescale. We obtain a set of equations in the variables $\{A_1, A_2, \varphi, \varphi_{\text{avg}} \equiv (\varphi_1 + \varphi_2)/2\}$:

$$A_1' = \frac{A_1}{2}(\beta\cos(\tau\omega) - \alpha) - \frac{3}{32}A_1\kappa\omega^2\big(A_2^2\cos(\tau\omega + 2\varphi) + \ldots$$
$$\ldots \quad 3A_1^2\cos(\tau\omega) + 2A_2^2\cos(\tau\omega)\big) \tag{30a}$$

$$A_2' = \frac{A_2}{2}(\beta\cos(\tau\omega) - \alpha) - \frac{3}{32}A_2\kappa\omega^2\big(A_1^2\cos(2\varphi - \tau\omega) + \ldots$$
$$\ldots \quad 2A_1^2\cos(\tau\omega) + 3A_2^2\cos(\tau\omega)\big) \tag{30b}$$

$$\varphi' = \frac{3}{16}\kappa\omega^2\sin(\varphi)\big(A_1^2\cos(\varphi - \tau\omega) + A_2^2\cos(\varphi + \tau\omega)\big) \tag{30c}$$

$$\varphi_{\text{avg}}' + \frac{\omega}{2} = \frac{\omega_0^2}{2\omega} - \frac{1}{2}\beta\sin(\tau\omega) + \frac{3}{64}\kappa\omega^2\big(A_2^2\sin(\tau\omega + 2\varphi) - \ldots$$
$$\ldots \quad A_1^2\sin(2\varphi - \tau\omega) + 5(A_1^2 + A_2^2)\sin(\tau\omega)\big) \tag{30d}$$

In (30), the first three equations describe the amplitudes and the synchronization of the two oscillators: the fixed points of these three equations in the three variables $\{A_1, A_2, \varphi\}$, which depend parametrically in ω, are the synchronized solutions of the system. The role of the last eq. (30d) will be explained in the next section §4.2.

For a fixed value of ω there are only two stable solutions among the fixed points of the system of equations (30a),(30b)

13

and (30c). These stable solutions are spinning waves and have amplitudes and phases:

$$\begin{cases} A_1 = & A_2 = \frac{2}{\sqrt{3}\omega}\sqrt{\frac{\beta - \alpha\sec(\tau\omega)}{\kappa}} \\ \varphi = & \pm\pi/2 \end{cases} \quad (31)$$

4.2. The choice of ω

We recall that ω defines the period $2\pi/\omega$ over which we carry out the time averaging, so that we should always choose ω to match the instantaneous frequency of oscillation of the oscillator in order to average exactly over one period of oscillation. When applying the method of averaging, one often assumes that the frequency of oscillation ω is close to the acoustic frequency of oscillation ω_0 of the unperturbed oscillator, and is approximately $\omega \approx \omega_0$. This assumption is often carried out earlier in the analysis, by fixing $\omega = \omega_0$ in (29). We have however observed in §3 that the frequency of oscillation ω_B of the neutrally stable, linearized system departs from ω_0, and is most noticeably dependent on τ, as in Fig. 3.b.

We can improve the choice of ω from ω_0 by using (30d), and choosing ω such that the mean average phase φ_{avg} is a fixed point of the system too. This also means that the frequency of averaging ω of the system matches the instantaneous frequency of the two oscillators, since we have that

$$\omega_{\mathrm{AVG}}^{\mathrm{inst}}(t) = \frac{\partial}{\partial t}\frac{(\omega t + \varphi_1(t)) + (\omega t + \varphi_2(t))}{2} = \omega + \varphi_{\mathrm{avg}}'(t) \quad (32)$$

This leads to an equation for ω:

$$\omega^2 = \omega_0^2 - \beta\omega\sin(\tau\omega) + \frac{3}{32}\kappa\omega^3\big(A_2^2\sin(\tau\omega + 2\varphi) - \dots$$
$$\dots \quad A_1^2\sin(2\varphi - \tau\omega) + 5(A_1^2 + A_2^2)\sin(\tau\omega)\big) \quad (33)$$

In the linear regime $A_i \to 0$, and from (33) we recover the linear dispersion relation (26b), with the difference that this time it is not calculated on the boundary of instability, i.e. (26a) does not hold.

In the general nonlinear regime before saturation, the frequency of oscillation shifts from the value ω solution of (33) and depends on the two amplitudes A_1 and A_2 and also on φ as described by (33). We numerically integrate in time the first three equations (30), and at each timestep calculate the instantaneous frequency ω, which satisfies (33). An example of a simulation is reported in Fig. 2, where A_1, A_2 and φ are reported as dotted lines.

In the nonlinear regime but at the converged limit cycle solution, we calculate the frequency ω_{LC} of oscillation at the limit cycle by substituting (31) into (33) and obtain:

$$h(\tau, \omega_{\mathrm{LC}}) \equiv \omega_{\mathrm{LC}}^2 - \omega_0^2 + \alpha\omega_{\mathrm{LC}}\tan(\omega_{\mathrm{LC}}\tau) = 0 \quad (34)$$

We find that (34), defining ω_{LC}, matches (27) defining ω_B, which is the frequency of the system on the boundary of linear stability obtained by suitably reducing the flame response of the unstable system to make it neutrally stable. We now show an example of the predictions of (32) in a time domain simulation.

To numerically integrate in time the system of equations (30), at each time step we numerically solve (33) for ω, and then calculate the right hand sides of (30) and proceed at the next time step. In Fig. 2.b we compare the instantaneous frequency ω as extracted from the original oscillators and the solution ω_{AVG} of (33) calculated as a function of the instantaneous amplitudes A_j. We have overall very good agreement, while we observe some small error in the fully linear and fully nonlinear regime.

In the fully linear regime at the left of Fig. 2.b the error between the frequency ω_{AVG} and the frequency of the linearized system is due to an inherent limitation of the method of averaging, which assumes that η_j and $\partial\eta_j/\partial t$ are exactly in quadrature. This is exact at the limit cycle if one neglects higher order harmonics, while the error made is largest where the growth rates are largest, which in this case is at the onset of oscillation. This error is however marginal and smaller than 0.02% in this time simulation. In the fully nonlinear regime at the right of Fig. 2.b the error between the frequency ω_{AVG} and the predicted frequency of oscillation ω_B is due to the fact that we are neglecting the contribution of higher order harmonics that in this case makes the amplitudes A_j just 1.5% smaller than the prediction A_{AVG} in Fig. 2.a. This in turn affects the amplitudes in (33), leading to an error however smaller than 0.02%.

We add a final note on the formal correctness of this derivation where the frequency of oscillation ω depends on time. The time-derivatives of $\{\eta_j, \eta_j'\}$ are $O(1)$ quantities i.e. are governed by time t. The method of averaging assumes that the slowly varying amplitudes and phases are $O(\varepsilon)$ quantities, i.e. are governed by time $T \equiv \varepsilon t$. In (B.1) we keep the terms that are $O(\varepsilon)$ i.e. we keep the time derivatives of the slow flow variables. In the mathematical derivations leading to (B.1), and more clearly in (32), we are implicitly assuming that the time derivative of ω can be neglected, i.e. we assume that $\partial\omega/\partial t$ is a term that scales with $O(\varepsilon^2)$ and neglect it. We present evidence that this approximation is reasonable in Fig. §2.b, where we observe that ω_{AVG} is rather close to the reconstructed value of ω especially in the regions where $\partial\omega/\partial t \neq 0$.

4.3. The method of multiple scales

We apply the method of multiple scales. We do not report the details of the derivation, which can be found in [90]. One obtains the set of equations:

$$A_1' = A_1\frac{L - \kappa N_A(A_1^2, A_2^2, +\varphi)}{D} \quad (35a)$$

$$A_2' = A_2\frac{L - \kappa N_A(A_2^2, A_1^2, -\varphi)}{D} \quad (35b)$$

$$\varphi' = \kappa\frac{N_\varphi(A_1^2, A_2^2, \varphi)}{D} \quad (35c)$$

$$\varphi_{\mathrm{avg}}' = \frac{N_{\varphi_{\mathrm{avg}}}(A_1^2, A_2^2, \varphi)}{2D} \quad (35d)$$

where the expressions of $L, N_A, N_\varphi, N_{\varphi_{\mathrm{avg}}}$ and D are reported in appendix §C, and the method predicts the instantaneous frequency of oscillation as

$$\omega_{\mathrm{MMS}}^{\mathrm{inst}}(t) = \omega_B + \varphi_{\mathrm{avg}}'(t) \quad (36)$$

In the first two equations, L/D is a linear growth coefficient and the term N_A/D is responsible for the nonlinear saturation of the amplitudes. The third equation governs the synchronization of the two oscillators, and depends only on nonlinear terms, since it is proportional to κ. The right hand side of (35d) is the frequency shift of the two oscillators, which depends on the amplitude of oscillation.

There are only two stable solutions among the fixed points of the system of equations (35a),(35b) and (35c) and they match exactly the solutions (31) of the method of averaging. The mean frequency of oscillation of the limit cycle is ω_B, because once we substitute (31) into (35d) we find that the numerator on the right hand side evaluates to zero. This means that the method of multiple scales predicts that the frequency of oscillation at the limit cycle equals ω_B, matching the prediction of the method of averaging.

For completeness, we present the instantaneous frequency of oscillation using the method of multiple scales as $\omega_{\mathrm{MMS}}(t)$ in Fig.2.b. The performance of this estimate is overall similar to the method of averaging, slightly better in the linear regime at small amplitudes.

4.4. Accuracy of the nonlinear solution

We tested the quality of these analytical solutions for a series of numerical simulations of (18) using the solver PYDELAY [91]. In particular we fix $\alpha/\omega = 0.08$ and run simulations of (18) on a fine grid with 153 values of β/α equispaced between 0 and 3 and 337 values of $\tau\omega_0$ equispaced between 0 and 8, for a total of 51561 simulations. We started the numerical integration at $t = 0$, with a history function defined for $t \in [0, -\tau]$, which is oscillatory. We then extract the amplitude and the frequency of the solutions once the numerical code has converged to a limit cycle. We report the amplitude in Fig. 7.a, and the frequency in Fig. 7.b. The agreement is overall very good, except for a small discrepancy at small values of β/α, where the contour line of the numerical solution at $A = 0.051$ is slightly jagged and slightly underpredicts the analytical solution in a few regions. This is due to the fact that we extracted the amplitudes from the numerical solutions too early in time, before the system had fully converged to the limit cycle. This is corroborated by the fact that for a constant α, smaller values of β/α make the system more weakly nonlinear, leading to longer time-scales for the evolution of the slow flow variables. On the horizontal line $\beta/\alpha = 3$ at the border of the investigated parameter space, where the system is more strongly nonlinear, the error between the predicted and measured amplitude was found to be smaller than 2.2%. On the same line, the error in the prediction of the frequency of oscillation was smaller than 0.08%.

4.5. The case of an axial mode

The averaged equations of (21) are obtained similarly:

$$A_1' = A_{1,\tau}\left[\nu - \delta A_{1,\tau}^2\right] \tag{37a}$$

$$\varphi_1' + \frac{\omega}{2} - \frac{\omega_0^2}{2\omega} = -\frac{\beta}{2}\sin(\tau\omega) + \delta\tan(\tau\omega)A_{1,\tau}^2 \tag{37b}$$

where we introduce

$$\begin{cases} \nu = (\beta\cos(\tau\omega) - \alpha)/2 \\ \delta = 3\kappa\cos(\tau\omega)\omega^2/8 \end{cases} \tag{38}$$

For reference, we observe that we can rewrite the right hand side of (37a) in terms of the flame describing function as $\mathrm{Re}[Q(A(t-\tau))]A(t-\tau)/2$ and similarly for (37b). Note how the amplitude A_1 on the right hand side of (37a) is delayed, i.e. $A_{1,\tau}(t) = A_1(t-\tau)$. In other words, we are not assuming here, as we did just after §4.1, that the delay τ is small compared to the time scale of A_1', because this section focuses in detail on the growth rate of A_1[7]. The limit cycle solution of the axial mode has the same amplitude A and the same frequency ω_B of the solution of the problem with two azimuthal modes[8]:

$$A = \sqrt{\frac{\nu}{\delta}} = \frac{2}{\sqrt{3}\omega_B}\sqrt{\frac{\beta - \alpha\sec(\tau\omega_B)}{\kappa}}$$

with ω_B solution of $h(\tau, \omega_L) = 0$ in (34). This means that the nonlinear results of Fig. 7.a apply also to a single mode.

4.6. Discussion

Using the method of averaging and the method of multiple scales we have obtained two sets of equations, respectively (30) and (35). Despite the fact that the two sets of equations differ, they share the same stable limit cycle solution, oscillating at the frequency ω_B of the neutrally stable system[9], and at the amplitude described by (31). This and the other results hold both for azimuthal and axial modes. As discussed in §4.4, the analytical solutions were validated against numerical simulations with excellent agreement, confirming that they characterize correctly the limit cycle solution. We present in Fig. 7 the amplitudes and frequencies of oscillation of the limit-cycle solution. As expected, in Fig. 7.a the amplitude grows from a value of 0 on the boundary of neutral stability as the ratio β/α increases along vertical lines of constant $\tau\omega_0$. Importantly, the smooth amplitude contour of the system in the nonlinear regime confirms that all the practical considerations discussed in §3 are still valid in the nonlinear regime.

We observe in Fig. 7.b that along vertical lines the frequency of oscillation at the limit cycle is constant, i.e. is independent of the flame strength β for a fixed level of acoustic damping α, as discussed also analytically in §4.2. This means that systems with different flame strengths β start at zero amplitude of oscillation with a different, linear frequency of oscillation ω_{lin} as in Fig. 2.b, but they all converge to the same frequency of oscillation ω_B. Note that we observe a frequency shift as a function of amplitude despite the fact that the flame phase does not depend on amplitude. This shift is small in the specific case of Fig. 2.b, but can be larger, and has been already observed in the literature: In particular [36, Fig. 8, first column] carry out a describing function limit cycle calculation and observe a shift

---

[7]Note that this does not affect any of the results of §4.1
[8]solutions for the two modes were presented in (31)
[9]defined as the solution of (26b)
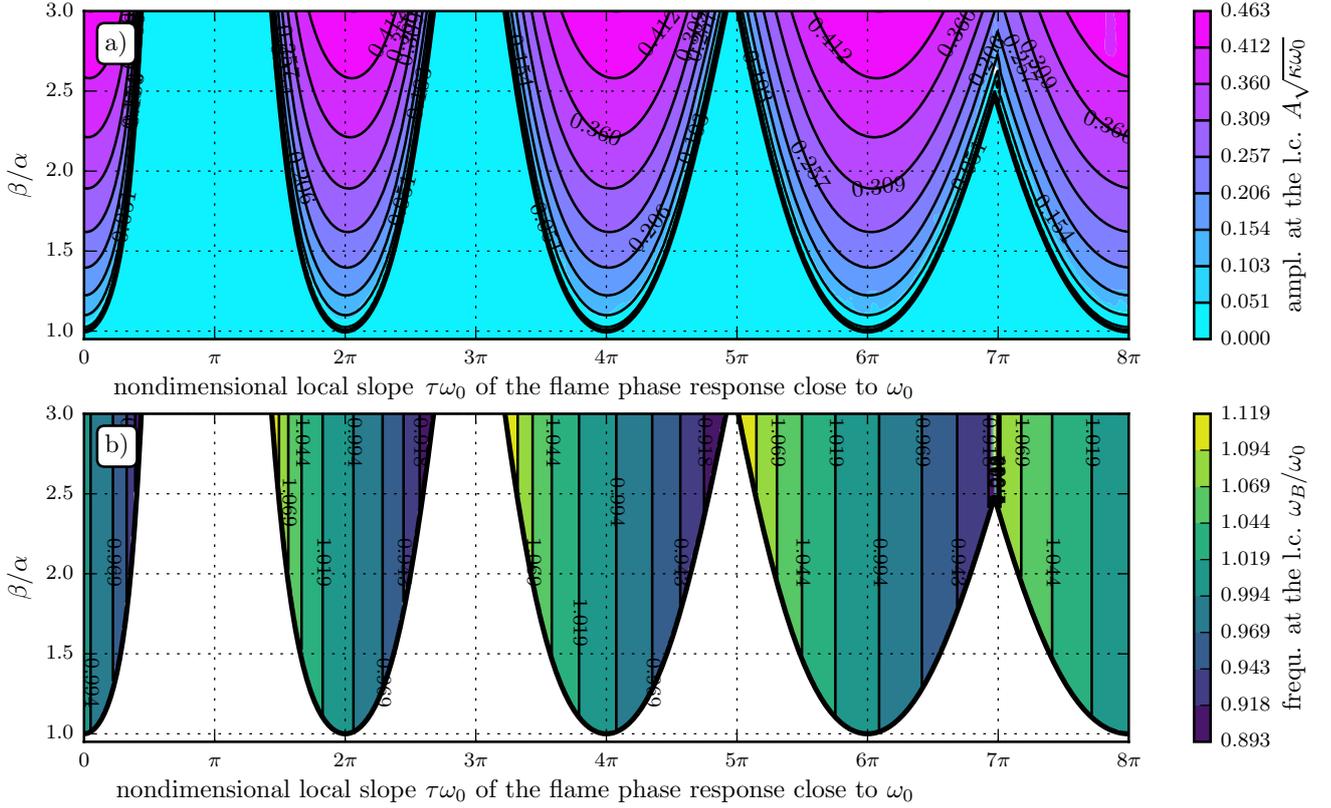
Figure 7: Nonlinear stability analysis of axial and azimuthal thermoacoustic modes characterized by an acoustic frequency of oscillation ω_0. a) Amplitude of oscillation $A\sqrt{\kappa\omega_0}$. b) Frequency of oscillation ω/ω_0. We compare the saturated amplitude and frequency at the limit cycle (l.c.) extracted from the numerical integration of the original system (18) (in colour) and of the analytical solution (black lines). In both a) and b) the black lines were chosen to be at the same levels as the colour contour boundaries. The two coincide almost exactly showing that the analytical solution matches the results of the numerical integration of the original system.

from the linear frequency to the limit cycle frequency up to 3%, in a range of frequencies where the flame phase is constant with amplitude [36, Fig. 2 at 145 Hz].

We have just discussed that ω_B does not depend on the flame strength β, but only on the level of acoustic damping α/ω_0 and on the phase response, as presented in Fig. 5 and 6. This has the physical interpretation that no matter how strong the flame response, pulsations will grow to an amplitude where the nonlinear gain of the flame balances the level of acoustic damping, which will be the same level obtained by reducing the flame strength to take the system onto the boundary of stability.

Both methods predict the evolution of the frequency of oscillation with time, as shown in Fig. 2.b. In the general case, sources (flames) and sinks (dampers) have a phase response that depends on the amplitude, leading to larger frequency shifts from the linear to the nonlinear regime. It is especially in these situations that one should take into account, in the time domain, the dependence of the frequency of oscillation on the amplitudes, as done here in (33).

5. Linear growth rate estimation

We have presented evidence at the end of §3 commenting on Fig. 3 of how neglecting the part of the heat release rate q not in phase with the pressure p as assumed in [47, 48] leads to systematic errors in the prediction of the boundary of stability and as a consequence of the amplitudes of oscillation. However, this assumption allows us to use a simplified model to identify the linear growth rate based on the pressure time series of a thermoacoustic system [48, 92]. One can then ask if the simplified model suffers the same systematic errors if it is used to identify a system instead of predicting its state, with a particular focus on the quantity of interest that is the linear growth rate. To this aim, in this section we show how the system of equations assumed by [92] with a zero delay τ, resembles in a certain mathematical sense the original system of equations with a non-zero delay τ. If this is the case, then one can safely use the methods discussed in [92] for linear growth rate estimation. We leave open the question of the identification of the delay τ and the case of azimuthal instabilities and focus on a thermoacoustic system with a single mode. We observe that the frequency of oscillation $\omega(t)$ is close to ω_B and in the following assume that $\omega(t) = \omega_B$ $\forall t$ in (37a) and discard the study of the equation for φ_1. [92] identifies a system of equations like (21) but with $\tau_{(E)}$ set to zero:

$$\eta_1''(t) + \omega_{0(E)}^2 \eta_1(t) = f(\eta_1'(t), \eta_1'(t-\tau)),$$
$$\text{with} \quad f(a) \equiv a(\beta_{(E)} - \kappa_{(E)} a^2) - \alpha a \quad (39a)$$

16

with the respective slow flow equation:

$$A_1' = A_1 \left[\nu_{(E)} - \delta_{(E)} A_1^2 \right] \tag{39b}$$

We then want to understand if there exists a set of coefficients $\{\nu_{(E)}, \delta_{(E)}, \omega_{0(E)}\}$ such that the dynamics of the equivalent (hence the subscript (E)) system (39b) matches the dynamics of the original system (37a), so that the system identification would identify it. We first observe that the frequency of oscillation of (39a) is well approximated by $\omega_{0(E)}$, so that it has to be $\omega_{0(E)} = \omega_B$. We then observe that in principle the dynamics of (37a) and (39b) cannot match because the first is of delayed differential type, while the second is of ordinary differential type. We can however approximate the Taylor expansion of the delayed term to the first order in τ:

$$A_{1,\tau} = A_1(t - \tau) \approx A_1(t) - \tau A_1'(t) + \mathcal{O}(\tau^2) \tag{40}$$

By substituting (40) into (37a) and after some manipulation we obtain:

$$A_1'(1 + \nu\tau - 3\delta\tau A_1^2) = \nu A_1 - \delta A_1^3 \tag{41}$$

Despite the fact that (41) does not have the same structure as (39b) in the nonlinear regime, one can expand in Maclaurin series the expression of A_1' in powers of A_1, truncate it to the third order, and match suitably the coefficients $\{\nu_{(E)}, \delta_{(E)}\}$. In the linear regime the two systems are equivalent:

$$\sigma^{(E)} = \nu_{(E)} \approx \frac{\nu}{1 + \tau\nu} \tag{42}$$

where $\sigma^{(E)}$ is the growth rate of (39a).

A similar argument can be applied with the method of multiple scales. In the linear regime the two modes A_1 and A_2 are decoupled in (35) and the linear coefficient matches the case of one thermoacoustic mode only. In this case the system is already of ordinary differential type, and one expects that

$$\sigma^{(E)} = \nu_{(E)} \approx \frac{L}{D} \tag{43}$$

We find good qualitative agreement in Fig. 8 between the exact growth rate of (21) in blue, the growth rate (42) in red, and the growth rate (43) in green, with the discrepancies to be attributed to the imperfect accuracy of the two nonlinear methods. As a comment, we observe in Fig. 8 a reduction as a function of $\tau\omega_0$ of all three growth rates. This effect of the delay τ can be observed in (42) and is additional to the direct effect of the phase $\tau\omega$ between q and p accounted for in the $\cos(\tau\omega)$ term in the definition (38) of ν. To conclude, we observe that equations (39) used by [92], with suitable coefficients $\{\nu_{(E)}, \delta_{(E)}\}$, match either the third order Maclaurin expansion of the equations (41) of the truncated method of averaging, or the equations of the method of multiple scales for one mode, assuming the approximation introduced by the truncation of the equations is acceptable. Then it follows that the system identification method [92] applied to timeseries of the original system (2.3) with delay should produce good growth rate estimates of the original system, within the limits of these approximations.

The mismatch in Fig. 8 shows that some of these approximations play a limited role.

This approximate equivalence between the models with and without delay is in line with past experience [43] with growth rate predictions on a model with a time delay, but requires further numerical evidence.

6. Conclusions

The aim of this work is to draw general conclusions about the stability[10] of thermoacoustic systems, by accounting for the fact that most flames have a response with a decreasing phase as function of the frequency ω, which can be approximated with a slope $-\tau$.

We find that the system's stability depends on the flame phase and gain as expected but also that steep phase responses, i.e. large values of τ, make the system more unstable, i.e. lead to an increase of the growth rate. This latter effect is closely related to how a thermoacoustic system can pulsate at a frequency ω_B different from the frequency ω_0 of the acoustic mode of the system that we focus on. In particular for a fixed frequency shift $\Delta\omega = \omega_B - \omega_0$, a steeper phase response leads to a larger phase change $\Delta\varphi = \tau\Delta\omega$ that in turn can make the Rayleigh term positive and the system unstable. We show that: *1)* flames with a steep flame phase are more likely to excite pulsations in a given combustor; *2)* a flame responding in anti-phase with the pressure at the flame location at the frequency ω_0 can still make the system unstable at a frequency $\omega \neq \omega_0$ in the neighbourhood of ω_0; *3)* a flame can destabilise an acoustic mode regardless of its phase at ω_0. For a given system characterized by a certain local phase slope τ in the vicinity of the frequency of oscillation ω_0, the quick calculation of $\tau\omega_0$ allows the estimation of the strength of the effect of the flame phase slope on the boundary of stability and amplitudes of the system.

We show how the model recovers frequency shifts that match typical experimental values, which are reviewed together with damping rates and growth rates for a selected set of references. Also the range of the phase ϕ_{qp} between heat release rate and acoustic pressure is close to experimental experience. In particular the model explains how ϕ_{qp} is an indicator of mode transition as proposed by [88]. We also present the interpretation of one transition between unstable/stable/unstable conditions with a strong frequency shift in the experiment of Boudy *et al.* [34].

We apply in the nonlinear regime the method of averaging and multiple scales. Both nonlinear methods lead to excellent results in the range of parameters that are typical of thermoacoustic oscillations when compared to numerical simulations. We prove that the results that apply in the nonlinear regime at the limit cycle match the results on the boundary of instability, obtained by suitably reducing the flame gain to the point of making the system neutrally stable. Both linear and nonlinear results apply to systems with either only one axial mode oscillating, or two degenerate azimuthal modes oscillating, where

---

[10]here and in the following, we use for brevity the term flame to mean the fluctuating heat release rate coming from the flame
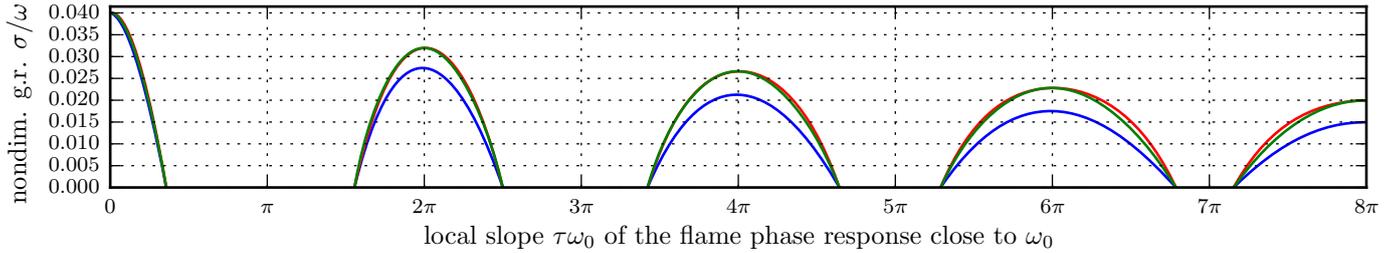
Figure 8: Linear growth rates (g.r.) of: the original equations of the system (2.3) with delay (blue), the truncated equations of the method of averaging (red), the equations of the method of multiple scales (green). These results are for $\beta/\alpha = 2, \alpha/\omega = 0.08$.

the coefficients in the equations differ in the two cases, as discussed first by [93].

We discuss also the sensitivity to the level of acoustic damping in the system. We find that, assuming the system saturation occurs because of nonlinear flame gain saturation, larger levels of acoustic damping lead to larger shifts of frequency at the limit cycle from the acoustic frequency ω_0. This effect is not governed by the flame gain because, regardless of its value in the nonlinear regime, it decreases up to the point of matching the level of acoustic damping.

We show that the part of flame response not in phase with the pressure at the flame location cannot be neglected when carrying out a prediction of the solution of a thermoacoustic system. This however does not imply that one must account for this component when identifying the linear growth rate of an observed thermoacoustic system. In an attempt to address this latter point, we present in §5 a conjecture suggesting that one may neglect this component when estimating the linear growth of a time series. A quantitative discussion of this conjecture will require further numerical validation.

Acknowledgements

[1] J. W. S. Rayleigh, The Explanation of Certain Acoustical Phenomena, Nature 18 (1878) 319–321.

[2] G. J. Bloxsidge, A. P. Dowling, N. Hooper, P. J. Langhorne, Active Control of Reheat Buzz, AIAA Journal 26 (1988) 783–790.

[3] F. Nicoud, T. Poinsot, Thermoacoustic instabilities : Should the Rayleigh criterion be extended to include entropy changes?, Combustion and Flame 142 (2005) 153–159.

[4] A. Gelb, W. Vander Velde, Multiple input describing functions and nonlinear system design, McGraw-Hill Book, 1968.

[5] S. Evesque, W. Polifke, Low-order acoustic modelling for annular combustors: validation and inclusion of modal coupling, Proceedings of ASME Turbo Expo 2002 (2002).

[6] G. A. Mensah, J. P. Moeck, Efficient computation of thermoacoustic modes in annular combustion chambers based on Bloch-wave theory, Proceedings of ASME Turbo Expo 2015, paper no. GT2015-43476 (2015) 1–11.

[7] D. Laera, G. Campa, S. M. Camporeale, A finite element method for a weakly nonlinear dynamic analysis and bifurcation tracking of thermoacoustic instability in longitudinal and annular combustors, Applied Energy 187 (2017) 216–227.

[8] C. Pankiewitz, T. Sattelmayer, Time Domain Simulation of Combustion Instabilities in Annular Combustors, Journal of Engineering for Gas Turbines and Power 125 (2003) 677–685.

[9] U. Krüger, J. Hüren, S. Hoffmann, W. Krebs, D. Bohn, Prediction of Thermoacoustic Instabilities With Focus on the Dynamic Flame Behavior for the 3A-Series Gas Turbine of Siemens KWU, in: Volume 2: Coal, Biomass and Alternative Fuels; Combustion and Fuels; Oil and Gas Applications; Cycle Innovations, ASME, Indianapolis (ID), U.S.A., 1999, pp. 1–11.

[10] S. R. Stow, A. P. Dowling, Thermoacoustic oscillations in an annular combustor, in: Proceedings of ASME Turbo Expo 2001. Paper no. GT2001-GT-0037, New Orleans, LS, USA, pp. 1–8.

[11] K. McManus, F. Han, W. Dunstan, C. Barbu, M. Shah, Modeling and Control of Combustion Dynamics in Industrial Gas Turbines, in: Proceedings of ASME Turbo Expo 2004, paper no. GT2004-53872, ASME, Vienna, Austria, 2004, pp. 1–9.

[12] J. Kopitz, A. Huber, T. Sattelmayer, W. Polifke, Thermoacoustic Stability Analysis of an Annular Combustion Chamber With Acoustic Low Order Modeling and Validation Against Experiment, in: Proceedings of ASME Turbo Expo 2005, paper no GT2005-68797, ASME, Reno (NV) U.S.A., 2005, pp. 1–11.

[13] J.-F. Bourgouin, D. Durox, J. P. Moeck, T. Schuller, S. Candel, Characterization and Modeling of a Spinning Thermoacoustic Instability in an Annular Combustor Equipped With Multiple Matrix Injectors, Journal of Engineering for Gas Turbines and Power 137 (2015) 021503.

[14] B. Schuermans, V. Bellucci, C. O. Paschereit, Thermoacoustic modeling and control of multi burner combustion systems, Proceedings of ASME Turbo Expo 2003 (2003).

[15] V. Bellucci, B. Schuermans, D. Nowak, P. Flohr, C. O. Paschereit, Thermoacoustic Modeling of a Gas Turbine Combustor Equipped With Acoustic Dampers, Journal of Turbomachinery 127 (2005) 372.

[16] S. R. Stow, A. P. Dowling, A Time-Domain Network Model for Nonlinear Thermoacoustic Oscillations, Journal of Engineering for Gas Turbines and Power 131 (2009) 031502.

[17] A. Orchini, S. J. Illingworth, M. P. Juniper, Frequency domain and time domain analysis of thermoacoustic oscillations with wave-based acoustics, Journal of Fluid Mechanics (2015) 387–414.

[18] A. P. Dowling, Nonlinear self-excited oscillations of a ducted flame, Journal of Fluid Mechanics 346 (1997) 271–290.

[19] J. P. Moeck, M. R. Bothien, S. Schimek, A. Lacarelle, C. O. Paschereit, Subcritical thermoacoustic instabilities in a premixed combustor, in: 14th AIAA/CEAS Aeroacoustics Conference, paper no. AIAA-2008-2946, AIAA, Vancouver (BC), Canada, 2008, pp. 2–18.

[20] A. Orchini, M. P. Juniper, Flame Double Input Describing Function analysis, Combustion and Flame 171 (2016) 87–102.

[21] W. Lang, T. Poinsot, S. Candel, Active Control of Combustion Instability, Combustion and Flame 70 (1987) 281–289.

[22] K. R. Mcmanus, T. Poinsot, S. M. Candel, A review of active control of combustion instabilities, Progress in Energy and Combustion Science 19 (1993) 1–29.

[23] A. P. Dowling, S. R. Stow, Acoustic Analysis of Gas Turbine Combustors, Journal of Propulsion and Power 19 (2003).

[24] T. Schuller, D. Durox, S. Candel, Self-induced combustion oscillations of laminar premixed flames stabilized on annular burners, Combustion and Flame 135 (2003) 525–537.

[25] D. Mejia, M. Miguel-Brebion, L. Selle, On the experimental determination of growth and damping rates for combustion instabilities, Combustion and Flame 169 (2016) 287–296.

[26] M. R. Bothien, J. P. Moeck, A. Lacarelle, C. O. Paschereit, Time domain modelling and stability analysis of complex thermoacoustic systems, Proceedings of the Institution of Mechanical Engineers, Part A: Journal of Power and Energy 221 (2007) 657–668.

[27] J.-F. Parmentier, P. Salas, P. Wolf, G. Staffelbach, F. Nicoud, T. Poinsot, A simple analytical model to study and control azimuthal instabilities in annular combustion chambers, Combustion and Flame 159 (2012) 2374–2387.

[28] G. Campa, M. Cinquepalmi, S. M. Camporeale, Influence of nonlinear flame models on sustained thermoacoustic oscillations in gas turbine combustion chambers, Proceedings of ASME Turbo Expo 2013, paper no. GT2013-94495 (2013) 1–13.

[29] M. Bauerheim, G. Staffelbach, N. A. Worth, J. R. Dawson, L. Y. Gicquel, T. Poinsot, Sensitivity of LES-based harmonic flame response model for turbulent swirled flames and impact on the stability of azimuthal modes, Proceedings of the Combustion Institute 35 (2015) 3355–3363.

[30] N. Noiray, D. Durox, T. Schuller, S. Candel, A unified framework for nonlinear combustion instability analysis based on the flame describing function, Journal of Fluid Mechanics 615 (2008) 139–167.

[31] E. Gullaud, S. Mendez, C. Sensiau, F. Nicoud, T. Poinsot, Effect of multi-perforated plates on the acoustic modes in combustors, Comptes Rendus Mécanique 337 (2009) 406–414.

[32] M. R. Bothien, J. P. Moeck, C. O. Paschereit, Comparison of Linear Stability Analysis With Experiments by Actively Tuning the Acoustic Premixed Combustor, Journal of Engineering for Gas Turbines and Power 132 (2010) 1–10.

[33] F. Nicoud, Application of modern tools for the acoustic study of annular combustion chambers, in: VKI Series Lectures - Advances in aeroacoustics and thermo-acoustics.

[34] F. Boudy, D. Durox, T. Schuller, G. Jomaas, S. Candel, Describing Function Analysis of Limit Cycles in a Multiple Flame Combustor, Journal of Engineering for Gas Turbines and Power 133 (2011) 061502.

[35] F. Boudy, D. Durox, T. Schuller, S. Candel, Nonlinear mode triggering in a multiple flame combustor, Proceedings of the Combustion Institute 33 (2011) 1121–1128.

[36] P. Palies, D. Durox, T. Schuller, S. Candel, Nonlinear combustion instability analysis based on the flame describing function applied to turbulent premixed swirling flames, Combustion and Flame 158 (2011) 1980–1991.

[37] P. Salas, Aspects numériques et physiques des instabilités thermoacoustiques dans les chambres de combustion annulaires, Ph.D. thesis, University of Bordeaux I, 2013.

[38] J. Schwing, T. Sattelmayer, High-Frequency Instabilities in Cylindrical Flame Tubes: Feedback Mechanism and Damping, in: Proceedings of ASME Turbo Expo 2003, paper no. GT2013-94064, volume 1A, ASME, San Antonio (TX), U.S.A., 2013, p. V01AT04A003.

[39] M. R. Bothien, N. Noiray, B. Schuermans, A Novel Damping Device for Broadband Attenuation of Low-Frequency Combustion Pulsations in Gas Turbines, Journal of Engineering for Gas Turbines and Power 136 (2013) 041504.

[40] C. F. Silva, F. Nicoud, T. Schuller, D. Durox, S. Candel, Combining a Helmholtz solver with the flame describing function to assess combustion instability in a premixed swirled combustor, Combustion and Flame 160 (2013) 1743–1754.

[41] M. Wagner, J. Christoph, T. Sattelmayer, Comparison of the accuracy of time-domain measurement methods for combustor damping, in: Proceedings of ASME Turbo Expo 2003, paper no. GT2013-94844, volume 1A, ASME, San Antonio (TX), U.S.A., 2013, pp. 1–11.

[42] N. Stadlmair, M. Wagner, C. Hirsch, T. Sattelmayer, Experimentally Determining the Acoustic Damping Rates of a Combustor With a Swirl Stabilized Lean Premixed Flame, in: Proceedings of ASME Turbo Expo 2015, paper no. GT2015-42683, ASME, Montreal, 2015, pp. 1–10.

[43] M. R. Bothien, N. Noiray, B. Schuermans, Analysis of Azimuthal Thermo-acoustic Modes in Annular Gas Turbine Combustion Chambers, Journal of Engineering for Gas Turbines and Power 137 (2015) 061505.

[44] G. Ghirardo, M. P. Juniper, J. P. Moeck, Weakly nonlinear analysis of thermoacoustic Instabilities in annular combustors, Journal of Fluid Mechanics 805 (2016) 52–87.

[45] E. Boujo, A. Denisov, B. Schuermans, N. Noiray, Quantifying acoustic damping using flame chemiluminescence, Journal of Fluid Mechanics 808 (2016) 245–257.

[46] N. Noiray, A. Denisov, A method to identify thermoacoustic growth rates in combustion chambers from dynamic pressure time series, Proceedings of the Combustion Institute 36 (2017) 3843–3850.

[47] B. Schuermans, C. O. Paschereit, P. Monkewitz, Non-Linear Combustion Instabilities in Annular Gas-Turbine Combustors, in: 44th AIAA

[48] Aerospace Sciences Meeting and Exhibit. Paper no. AIAA-2006-0549, American Institute of Aeronautics and Astronautics, Reno (NV), U.S.A., 2006, pp. 1–12.

[48] N. Noiray, M. R. Bothien, B. Schuermans, Investigation of azimuthal staging concepts in annular gas turbines, Combustion Theory and Modelling 15 (2011) 585–606.

[49] J. P. Moeck, C. O. Paschereit, Nonlinear interactions of multiple linearly unstable thermoacoustic modes, International Journal of Spray and Combustion Dynamics 4 (2012).

[50] L. Kabiraj, A. Saurabh, P. Wahi, R. I. Sujith, Route to chaos for combustion instability in ducted laminar premixed flames., Chaos 22 (2012).

[51] H. Gotoda, M. Amano, T. Miyano, T. Ikawa, K. Maki, S. Tachibana, Characterization of complexities in combustion instability in a lean premixed gas-turbine model combustor, Chaos: An Interdisciplinary Journal of Nonlinear Science 22 (2012) 043128.

[52] K. Kashinath, I. C. Waugh, M. P. Juniper, Nonlinear self-excited thermoacoustic oscillations of a ducted premixed flame: bifurcations and routes to chaos, Journal of Fluid Mechanics 761 (2014) 399–430.

[53] M. Hoeijmakers, V. Kornilov, I. Lopez Arteaga, P. de Goey, H. Nijmeijer, Intrinsic instability of flameacoustic coupling, Combustion and Flame 161 (2014) 2860–2867.

[54] T. Emmert, S. Bomberg, W. Polifke, Intrinsic thermoacoustic instability of premixed flames, Combustion and Flame 162 (2015) 75–85.

[55] G. Ghirardo, M. P. Juniper, Azimuthal instabilities in annular combustors: standing and spinning modes, Proceedings of the Royal Society A: Mathematical, Physical and Engineering Sciences 469 (2013) 20130232.

[56] B. Ćosić, J. P. Moeck, C. O. Paschereit, Nonlinear Instability Analysis for Partially Premixed Swirl Flames, Combustion Science and Technology 186 (2014) 713–736.

[57] T. Schuller, N. Tran, N. Noiray, D. Durox, S. Ducruix, S. Candel, The role of nonlinear acoustic boundary conditions in combustion/acoustic coupled instabilities, in: Proceedings of ASME Turbo Expo 2009, paper no. GT2009-59390, pp. 1–15.

[58] J. P. Moeck, M. Paul, C. O. Paschereit, Thermoacoustic instabilities in an annular Rijke tube, Proceedings of ASME turbo expo 2010, paper no. GT2010-23577 (2010).

[59] P. Wolf, G. Staffelbach, R. Balakrishnan, A. Roux, T. Poinsot, Azimuthal instabilities in annular combustion chambers, in: Center for Turbulence research, Proceedings of the Summer program, pp. 259–269.

[60] M. Bauerheim, J.-F. Parmentier, P. Salas, F. Nicoud, T. Poinsot, An analytical model for azimuthal thermoacoustic modes in an annular chamber fed by an annular plenum, Combustion and Flame 161 (2014) 1374–1389.

[61] V. Acharya, D.-h. Shin, T. Lieuwen, Premixed Flames Excited by Helical Disturbances: Flame wrinkling and heat release oscillations, Journal of Propulsion and Power 29 (2013).

[62] A. Saurabh, J. P. Moeck, C. O. Paschereit, Swirl Flame Response to Simultaneous Axial and Transverse Velocity Fluctuations, Journal of Engineering for Gas Turbines and Power 139 (2017) 061502.

[63] A. Saurabh, C. O. Paschereit, Dynamics of premixed swirl flames under the influence of transverse acoustic fluctuations, Combustion and Flame 182 (2017) 298–312.

[64] T. Lieuwen, B. T. Zinn, The role of equivalence ratio oscillations in driving combustion instabilities in low NOx gas turbines, International Symposium on Combustion 27 (1998) 1809–1816.

[65] W. Polifke, J. Kopitz, A. Serbanoviv, Impact of the fuel time lag distribution in elliptical premix nozzles on combustion stability, in: 7th AIAA/CEAS Aeroacoustics Conference and Exhibit, May, American Institute of Aeronautics and Astronautics, Reston, Virigina, 2001, pp. 1–11.

[66] V. Bellucci, B. Schuermans, C. O. Paschereit, P. Flohr, Thermoacoustic simulation of lean premixed flames using an enhanced time-lag model, in: 15th AIAA Computational Fluid Dynamics Conference, paper no. 2001-2794, American Institute of Aeronautics and Astronautics, Anaheim (CA) U.S.A., 2001, pp. 1–7.

[67] W. Krebs, P. Flohr, B. Prade, S. Hoffmann, Thermoacoustic stability chart for high-intensity gas turbine combustion systems, Combustion science and Technology 174 (2002) 99–128.

[68] M. Fleifil, A. M. Annaswamy, Z. A. Ghoneim, A. F. Ghoniem, Response of a Laminar Premixed Flame to Flow Oscillations : A Kinematic Model and Thermoacoustic Instability Results, Combustion and Flame 106 (1996) 487–510.

[69] S. Ducruix, D. Durox, S. Candel, Theoretical and experimental determi-

nations of the transfer function of a laminar premixed flame, Proceedings of the Combustion Institute 28 (2000) 765–773.

[70] Preetham, H. Santosh, T. Lieuwen, Dynamics of Laminar Premixed Flames Forced by Harmonic Velocity Disturbances, Journal of Propulsion and Power 24 (2008) 1390–1402.

[71] P. Palies, D. Durox, T. Schuller, S. Candel, The combined dynamics of swirler and turbulent premixed swirling flames, Combustion and Flame 157 (2010) 1698–1717.

[72] B. Schuermans, W. Polifke, C. O. Paschereit, Modeling transfer matrices of premixed flames and comparison with experimental results, ASME, International Gas Turbine and Aeroengine Congress and Exhibition, Indianapolis, IN (1999).

[73] B. Schuermans, V. Bellucci, F. Güthe, F. Meili, P. Flohr, C. O. Paschereit, A detailed analysis of thermoacoustic interaction mechanisms in a turbulent premixed flame, in: Proceedings of ASME Turbo Expo 2004, paper no. GT2004-53831, Vienna, Austria, pp. 539–551.

[74] T. Lieuwen, Modeling Premixed Combustion-Acoustic Wave Interactions: A Review, Journal of Propulsion and Power 19 (2003) 765–781.

[75] S. Candel, D. Durox, T. Schuller, J.-F. Bourgouin, J. P. Moeck, Dynamics of Swirling Flames, Annual Review of Fluid Mechanics 46 (2014) 147–173.

[76] W. Krebs, S. Hoffmann, B. Prade, M. Lohrmann, H. Büchner, Thermoacoustic Flame Response of Swirl Flames, in: Proceedings of ASME Turbo Expo 2002, paper no. GT-2002-30065, Amsterdam, Netherlands, pp. 1–12.

[77] G. Ghirardo, B. Ćosić, M. P. Juniper, J. P. Moeck, State-space realization of a describing function, Nonlinear Dynamics 82 (2015) 9–28.

[78] S. K. Thumuluru, H.-h. Ma, T. Lieuwen, Measurements of the Flame Response to Harmonic Excitation in a Swirl Combustor, in: 45th AIAA Aerospace Sciences Meeting and Exhibit, paper no. AIAA 2007-845, Reno (NV) U.S.A., pp. 1–15.

[79] P. Subramanian, R. I. Sujith, P. Wahi, Subcritical bifurcation and bistability in thermoacoustic systems, Journal of Fluid Mechanics 715 (2013) 210–238.

[80] G. Campa, S. M. Camporeale, Influence of nonlinear effects on the limit cycle in a combustion chamber equipped with Helmholtz resonator, Proceedings of ASME Turbo Expo 2014, paper no. GT2014-25228 (2014) 1–11.

[81] R. Balachandran, A. P. Dowling, E. Mastorakos, Non-linear Response of Turbulent Premixed Flames to Imposed Inlet Velocity Oscillations of Two Frequencies, Flow, Turbulence and Combustion 80 (2008) 455–487.

[82] C. Armitage, R. Balachandran, E. Mastorakos, R. Cant, Investigation of the nonlinear response of turbulent premixed flames to imposed inlet velocity oscillations, Combustion and Flame 146 (2006) 419–436.

[83] N. Noiray, B. Schuermans, Deterministic quantities characterizing noise driven Hopf bifurcations in gas turbine combustors, International Journal of Non-Linear Mechanics 50 (2013) 152–163.

[84] N. Noiray, Linear Growth Rate Estimation From Dynamics and Statistics of Acoustic Signal Envelope in Turbulent Combustors, Journal of Engineering for Gas Turbines and Power 139 (2017).

[85] G. Bonciolini, E. Boujo, N. Noiray, Effects of turbulence-induced colored noise on thermoacoustic instabilities in combustion chambers, in: International Symposium: Thermoacoustic Instabilities in Gas Turbines and Rocket Engines, May 30 - June 02, 2016 Munich (DE), pp. 1–11.

[86] J. H. I. Crawford, T. Lieuwen, Time Delay and Noise Coupling in Limiting Control Effectiveness in Unstable Combustors, in: 48th AIAA Aerospace Sciences Meeting Including the New Horizons Forum and Aerospace Exposition, paper no. AIAA 2010-1519, AIAA, Orlando (FL), U.S.A., 2010, pp. 1–16.

[87] D. Durox, T. Schuller, N. Noiray, A. Birbaud, S. Candel, Rayleigh criterion and acoustic energy balance in unconfined self-sustained oscillating flames, Combustion and Flame 156 (2009) 106–119.

[88] S. Hong, S. J. Shanbhogue, R. L. Speth, A. F. Ghoniem, On the phase between pressure and heat release fluctuations for propane / hydrogen flames and its role in mode transitions, Combustion and Flame 160 (2013) 2827–2842.

[89] J. A. Sanders, F. Verhulst, Averaging Methods in Nonlinear Dynamical Systems, volume 59 of *Applied Mathematical Sciences*, Springer, 2nd edition, 2007.

[90] G. Ghirardo, Nonlinear analysis of thermoacoustic modes in axisymmetric annular combustors, Ph.D. thesis, University of Cambridge, 2016.

[91] V. Flunkert, E. Schoell, Pydelay - a python tool for solving delay differential equations, ArXiv (2009).

[92] N. Noiray, Linear growth rate estimation from dynamics and statistics of acoustic signal envelope in turbulent combustors, in: Proceedings of the ASME TurboExpo 2016 paper no. GT2016-58169, pp. 1–11.

[93] L. Crocco, Research on combustion instability in liquid propellant rockets, Symposium (International) on Combustion 12 (1969) 85–99.

[94] P. Wahi, A. Chatterjee, Averaging Oscillations with Small Fractional Damping and delayed terms, Nonlinear dynamics 38 (2004) 3–22.

[95] A. Saha, B. Bhattacharya, P. Wahi, A comparative study on the control of friction-driven oscillations by time-delayed feedback, Nonlinear Dynamics 60 (2010) 15–37.

Appendices

A. Mathematical derivation of the linear stability analysis

By studying as a function of σ the left and right hand sides of (25a) for fixed values of the other parameters in the discussed ranges, we find that there exists only one solution for the growth rate σ, and that it is positive if $\beta \cos(\tau\omega) - \alpha > 0$. It follows that (26a) defines the boundary of stability, with the system being unstable if the left hand side is positive. We also observe from (26b) that on the boundary, if τ is zero, ω_B matches the acoustic frequency of oscillation ω_0. We observe that if (α, β, τ) provide a real-valued solution ω_B of (26), then (α, β, τ_k) is a solution too, with

$$\tau_k = \tau + 2k\pi/\omega_B \ , \qquad k \in \mathbb{N}^+. \tag{A.1}$$

We can then initially limit the search of solutions restricting the domain of τ to

$$\tau \in \left[-\frac{\pi}{\omega_B}, \frac{\pi}{\omega_B} \right) \tag{A.2}$$

and then exploit (A.1) to generate the other solutions. Since ω_B is close to the natural frequency of the system, ω_0, the domain (A.2) is bounded. Moreover, since α and β are positive, (26a) allows us to further restrict the domain so that the cosine term is positive:

$$\tau \in \left[-\frac{\pi}{2\omega_B}, \frac{\pi}{2\omega_B} \right) \tag{A.3}$$

This is in line with the Rayleigh criterion [1]: the phase difference between q and p must be in the range $(-\pi/2, \pi/2)$ to maintain or sustain instability.

The domain (A.3) allows negative values of τ, though a negative value in the system does not make physical sense. We investigate negative solutions nonetheless, because they lead to positive solutions τ_k by the application of (A.1). The neutrality of the solutions is defined by (26a), from which we can calculate the linear driving β_L at the onset of instability as a function of α and τ:

$$\beta_L = \alpha \sec(\tau\omega_B), \tag{A.4}$$

The frequencies of the neutrally stable solutions are the solutions ω_B of (26b). We substitute β from (A.4) into (26b) and obtain:

$$h(\tau\omega_0, \omega_B/\omega_0) \equiv \omega_B^2 - \omega_0^2 + \alpha\omega_B \tan(\tau\omega_B) = 0 \quad \text{(A.5)}$$

We can solve $\tau\omega_0$ as function of ω_B/ω_0 parametrically in the level of damping α/ω_0:

$$\tau\omega_0 = \left(\frac{\omega_B}{\omega_0}\right)^{-1} \arctan\left(\frac{1 - \left(\frac{\omega_B}{\omega_0}\right)^2}{\frac{\alpha}{\omega_0}\frac{\omega_B}{\omega_0}}\right) \quad \text{(A.6)}$$

reported in Fig. A.1. There are two solutions ω_B for each value of τ if $\hat{\tau} < \tau < 0$, with $\hat{\tau}\omega_0 \approx -1.13$. This line shows the effect of $\tau\omega_0$ on the frequency shift, ω_B/ω_0, on the border of neutral stability. We present in Fig. A.2.a the curve for
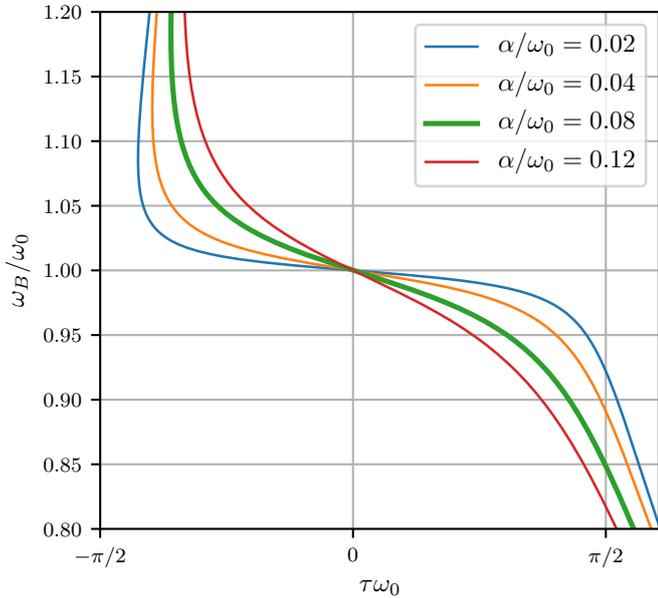
Figure A.1: Curves (A.6) for different values of the nondimensional damping α/ω, zoomed in to the approximate range for ω for thermoacoustic applications fixed to $\omega_0 \pm 20\%$. In the following we use $\alpha/\omega = 0.08$.

$\alpha/\omega_0 = 0.08$, but colour it based on the value of the ratio β/α that makes the system neutrally stable calculated using (A.4) and zoom to the range of parameters typical of thermoacoustic applications discussed in §2.4. We present in Fig. A.2.b the same information but invert the vertical axis and the colourmap. We mention how similar plots for liquid propellant rockets date back at least to [93, Fig. 1].

We then recover the full boundary of neutral stability by applying the transformation (A.1) to values of $(\beta/\alpha, \tau\omega_0)$ from Fig. A.2 and present it in Fig. 3. In Fig. 3.a the lobe/trough with a minimum at $\tau\omega_0 = 2\pi$ is obtained for $k = 1$ in (A.1), the lobe/trough with a minimum at 4π is obtained for $k = 2$ in (A.1) and so on so forth. The mapping (A.1) is key to interpret how the boundary of stability is deformed as function of k. In particular one sees that if $\omega_B = \omega_0$, the point $\tau\omega_0$ is simply

mapped to $\tau\omega_0 + 2k\pi$, in a periodic fashion. Then, if $\omega_B < \omega_0$, the point is mapped to a larger value than $\tau\omega_0 + 2k\pi$, and if $\omega_B > \omega_0$ it is mapped to a smaller value of $\tau\omega_0 + 2k\pi$.

A.1. Results obtained neglecting the imaginary part of the describing function

For comparison with the previous work of [47, 48], we now make the same assumption and set to zero the part of the heat release rate q out of phase with p, i.e. the $\sin(.)$ term appearing in equations (26b). The equations (26) simplify to

$$\beta\cos(\tau\omega_B) - \alpha = 0 \quad \text{(A.7a)}$$
$$\omega_B^2 - \omega_0^2 = 0 \quad \text{(A.7b)}$$

In equations (A.7) we find that regardless of the values of α, β and τ the linear frequency of oscillation at the neutral boundary of stability coincides with the natural acoustic frequency of the unperturbed oscillator:

$$\begin{cases} \beta &= \alpha/\cos(\tau\omega_0) \\ \omega_B &= \omega_0 \end{cases} \quad \text{(A.8)}$$

These results are presented in Fig. A.2 and 3 with black lines.

A.2. Generalization for $\psi \equiv \phi_0 + \tau\omega_0 \neq 0$

We can rewrite (15) as

$$\frac{\hat{q}(\omega)}{\hat{p}(\omega)} = \beta e^{i(\psi - \tau\omega)} \quad \text{for } \omega \text{ close to } \omega_0, \psi \in [-\pi, \pi) \quad \text{(A.9)}$$

where

$$\psi = \phi_0^\psi + \tau^\psi\omega_0 \quad \text{(A.10)}$$

One looks for the solution of (26) where the additional term $-\psi$ appears in the equations:

$$\beta\cos(\tau\omega_B - \psi) - \alpha = 0 \quad \text{(A.11a)}$$
$$\omega_B^2 - \omega_0^2 + \beta\omega_B \sin(\tau\omega_B - \psi) = 0 \quad \text{(A.11b)}$$

One can generate a solution for (A.11) from the solution of (26). In particular, we observe that if $\{\alpha, \beta, \tau^{\psi=0}\omega_0\}$ lead to a neutrally stable frequency ω_B/ω_0 in (26), then $\{\alpha, \beta, \tau^\psi\omega_0\}$ lead to the same frequency ω_B/ω_0 if:

$$\tau^{\psi=0}\omega_B = \tau^\psi\omega_B - \psi \quad \text{(A.12)}$$

We substitute in (A.12) the expression (A.10) for ψ and obtain:

$$\tau^{\psi=0}\omega_B = \tau^\psi(\omega_B - \omega_0) - \phi_0 \quad \text{(A.13)}$$

We now observe from (A.10) that

$$\phi_0^{\psi=0} = -\tau^{\psi=0}\omega_0 \quad \text{(A.14)}$$

We manipulate the left hand side of (A.13), and substitute (A.14) to obtain

$$\tau^{\psi=0}\omega_B = \tau^{\psi=0}\omega_0 + \tau^{\psi=0}(\omega_B - \omega_0) \quad \text{(A.15)}$$
$$= -\phi_0^{\psi=0} + \tau^{\psi=0}(\omega_B - \omega_0) \quad \text{(A.16)}$$
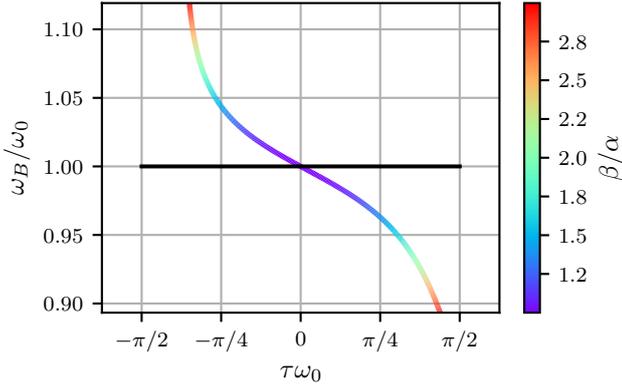
(a) frequency of neutral stability
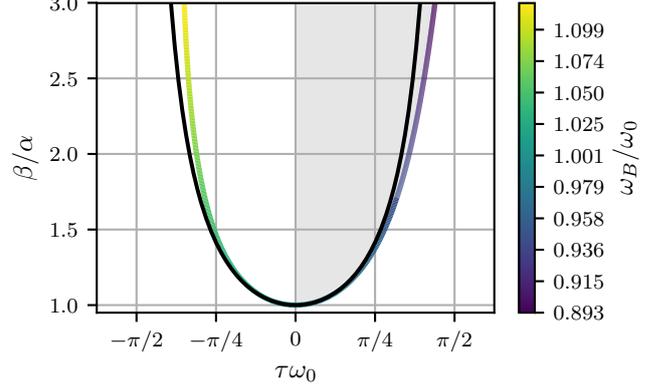
(b) ratio β/α of driving over damping at neutral stability

Figure A.2: Linear stability analysis, carried out parametrically as a function of the local slope $\tau\omega_0$. a) The coloured line is the frequency of the neutrally stable modes as a function of $\tau\omega_0$. This is the line for $\alpha/\omega_0 = 0.08$ presented first in Fig. A.1, but coloured with the values of β/α that make the system neutrally stable. b) stability map of the system. This is the same data of a) but swapping the vertical axis with the colourmap. The coloured line represents the values of β/α as a function of τ on which the system is neutrally stable. We study the system for positive values of $\tau\omega_0$, where the linearly unstable region is reported in grey. The same analysis on the system obtained by neglecting the component of q not in phase with p as done in [47, 48] is reported with black lines in frames a) and b)

Finally, by moving the terms between the two sides, (A.13) becomes

$$\phi_0^\psi - \phi_0^{\psi=0} = \left(\frac{\omega_B}{\omega_0} - 1\right)\left(\tau^\psi\omega_0 - \tau^{\psi=0}\omega_0\right) \quad (A.17)$$

Equation (A.17) shows that one point $(\tau^{\psi=0}\omega_0, \beta/\alpha)$ of the boundary of stability of Fig. 3, which has a flame phase at $\omega = \omega_0$ expressed by (A.14), is mapped in the general case to a line with slope $\omega_B/\omega_0 - 1$. We draw these lines of neutral stability in red in Fig. 5 for different values of the ratio of β/α. In particular for each value of the ratio β/α there are two lines, one with positive and one with negative slope. A point $(\tau\omega, \phi_0)$ is linearly unstable if it is between these two lines, linearly stable otherwise. In the same figure we plot also in colour the ratio ω_B/ω_0, which is constant along these lines, with the colourbar on the right.

The phase between heat release rate and the pressure is the argument of the complex exponential in (15):

$$\phi_{qp} = \phi_0^\psi - \tau^\psi(\omega - \omega_0) \quad (A.18)$$

$$= \phi_0^\psi - \tau^\psi\omega_0\left(\frac{\omega_B}{\omega_0} - 1\right) \quad (A.19)$$

We remind the reader that ϕ_{qp} is the flame phase at the frequency $\omega = \omega_B$ of the thermoacoustic mode, which does not match ϕ_0 because the latter is the flame phase calculated at $\omega = \omega_0$. The phase ϕ_{qp} is presented in Fig. 5.b.

B. Mathematical aspects of the method of averaging

We substitute (29) into (28), and add (28a) multiplied by $ie^{i(\omega t+\varphi_j)}\omega$ and (28b) multiplied by $-e^{i(\omega t+\varphi_j)}$. We obtain

$$\frac{\omega^2 - \omega_0^2}{2}A_j e^{2i(\omega t+\varphi_j(t))} + \omega\left(\varphi_i'(t) + \frac{\omega}{2} - \frac{\omega_0^2}{2\omega}\right)A_j(t) + \dots$$

$$\dots i\omega A_j'(t) = -e^{i(\omega t+\varphi_j(t))}f_j(t, A_1(t), A_1(t), \dots) \quad (B.1)$$

where f depends on the fast time variable t and on the slow variables, which are the amplitudes $A_1(t), A_2(t), A_1(t-\tau), A_2(t-\tau)$ and the phases $\varphi_1(t), \varphi_2(t), \varphi_1(t-\tau), \varphi_2(t-\tau)$. Note that f is periodic in its direct dependence on t, with period $2\pi/\omega$. We apply first order averaging as discussed by [89]: we approximate the slow variables as constant in the period of oscillation $2\pi/\omega$ and time-average both sides of (B.1). The first term on the left hand side has period π/ω and vanishes. We are left with:

$$\left(\varphi_i'(t) + \frac{\omega}{2} - \frac{\omega_0^2}{2\omega}\right)A_j(t)\omega + i\omega A_j'(t) \approx \quad (B.2)$$

$$-\frac{1}{2\pi/\omega}\int_{t-\pi/\omega}^{t+\pi/\omega}e^{i(\omega s+\varphi_j(t))}f_j(s, A_1(t), \dots)ds$$

In the integral on the right hand side, the delayed slow variables such as $A_1(t-\tau)$ are approximated as $A_1(t)$ since the delay τ is assumed to be of the same order as the period of oscillation, i.e. small compared to the time scale of the slow variables, as discussed by [94, 95]. We will relax this assumption later in §5.

We then evaluate the right hand side RHS$_j$ of (B.2). We take the constant term $e^{i\varphi_j(t)}$ out of the integral, introduce the point $z = e^{i\omega s}$ on the complex unit circle and change the integration variable from s to z, obtaining a closed path integral on the unit circle around the origin:

$$\text{RHS}_j = -e^{i\varphi_j(t)}\frac{1}{2\pi i}\oint f_j(z, A_1(t), \dots)dz$$

$$= -e^{i\varphi_j(t)}\text{Res}_{z=0}[f_j] \quad (B.3)$$

The term $f_j(z, A_1(t), \dots)$ is a Laurent polynomial in z, and is then holomorphic everywhere except at $z = 0$, so that in the last passage above we applied the residue theorem. The residue is the coefficient of $1/z$ in the expression of f_j. The right hand

side of (B.2) divided by ω for $j = 1$ evaluates to

$$g(A_1, A_2, \varphi) \equiv \frac{\text{RHS}_1}{\omega} = -\frac{e^{i\varphi_1(t)}}{\omega}\text{Res}_{z=0}[f_1] \qquad \text{(B.4a)}$$

$$= \frac{1}{2}iA_1\left(\beta e^{i\tau\omega} - \alpha\right) - \quad \ldots$$

$$\ldots \quad \frac{3}{32}iA_1\kappa\omega^2 e^{i\tau\omega}\left(A_2^2 e^{2i\varphi} + 3A_1^2 + 2A_2^2\right)$$

where φ is the difference between the phases of the first and second oscillator, $\varphi \equiv \varphi_1 - \varphi_2$, and the expression for g_2 is obtained similarly. In particular one finds

$$\frac{\text{RHS}_2}{\omega} = g(A_2, A_1, -\varphi) \qquad \text{(B.4b)}$$

We divide both sides of (B.2) by ω, substitute (B.4), and obtain the equations for the time evolution of the slow variables of the two oscillators:

$$\left(\varphi_1'(t) + \frac{\omega}{2} - \frac{\omega_0^2}{2\omega}\right)A_1(t) + iA_1'(t) = g(A_1, A_2, +\varphi) \qquad \text{(B.5a)}$$

$$\left(\varphi_2'(t) + \frac{\omega}{2} - \frac{\omega_0^2}{2\omega}\right)A_2(t) + iA_2'(t) = g(A_2, A_1, -\varphi) \qquad \text{(B.5b)}$$

with $\varphi \equiv \varphi_1 - \varphi_2$. This dynamical system is in terms of the variables $\{A_1, A_2, \varphi_1, \varphi_2\}$ and can present solutions where both phases φ_1 and φ_2, in the limit $t \to \infty$, present a common oblique asymptote, i.e. the two oscillators undergo the same shift of their oscillation frequency. However, these solutions are not fixed points of (B.5) since $\varphi_j'(t) \neq 0$. These solutions are however fixed points of an equivalent system, in terms of the variables $\boldsymbol{x} = \{A_1, A_2, \varphi, \varphi_{\text{avg}} \equiv (\varphi_1 + \varphi_2)/2\}$, which is presented in (30).

C. Slow flow equations for the method of multiple scales

We report in (C.1) the expressions introduced in (35) and obtained with the method of multiple scales:

$$D = 16\left(\alpha^2 + \left(4(\alpha\tau + 1)\omega_L^2 - \alpha^2\right)\cos(2\tau\omega_L) + 2(\alpha\tau(\alpha\tau + 2) + 2)\omega_L^2 + 2\alpha(\alpha\tau + 2)\omega_L\sin(2\tau\omega_L)\right)$$

$$L = -16\omega_L\left(\alpha - \beta\cos(\tau\omega_L)\right)\left(\alpha\sin(2\tau\omega_L) + 2\omega_L\left(\alpha\tau + \cos(2\tau\omega_L) + 1\right)\right) \qquad \text{(C.1a)}$$

$$N_A(A_1^2, A_2^2, \varphi) = 3\omega_L^3\Big(2\omega_L\left(A_2^2\cos(2\varphi) + 3A_1^2 + 2A_2^2\right)\cos(\tau\omega_L)\left(\alpha\tau + \cos(2\tau\omega_L) + 1\right)$$

$$+ \sin(2\tau\omega_L)\left(\cos(\tau\omega_L)\left(\alpha A_2^2\cos(2\varphi) + 3\alpha A_1^2 + 2\alpha A_2^2 - 2A_2^2\omega_L\sin(2\varphi)\right)\right.$$

$$\left.- \alpha A_2^2\sin(2\varphi)\sin(\tau\omega_L)\right)\Big) \qquad \text{(C.1b)}$$

$$N_\varphi(A_1^2, A_2^2, \varphi) = 6\omega_L^3\sin(\varphi)\cos(\tau\omega_L)\Big(2\left(A_1^2 - A_2^2\right)\sin(\varphi)\sin(\tau\omega_L)\left(\alpha\sin(\tau\omega_L) + 2\omega_L\cos(\tau\omega_L)\right)$$

$$+ \left(A_1^2 + A_2^2\right)\cos(\varphi)\left(\alpha\sin(2\tau\omega_L) + 2\omega_L\left(\alpha\tau + \cos(2\tau\omega_L) + 1\right)\right)\Big) \qquad \text{(C.1c)}$$

$$N_{\varphi_{\text{avg}}}(A_1^2, A_2^2, \varphi) = \omega_L\Big(\sin(2\tau\omega_L)\left(\alpha\sin(\tau\omega_L) + 2\omega_L\cos(\tau\omega_L)\right)\left(15\left(A_1^2 + A_2^2\right)\kappa\omega_L^2 - 32\beta + 32\alpha\sec(\tau\omega_L)\right)$$

$$+ 3\left(A_1^2 + A_2^2\right)\kappa\omega_L^2\cos(2\varphi)\sin(2\tau\omega_L)\left(\alpha\sin(\tau\omega_L) + 2\omega_L\cos(\tau\omega_L)\right)$$

$$- 3\left(A_1^2 - A_2^2\right)\kappa\omega_L^2\sin(2\varphi)\cos(\tau\omega_L)\left(\alpha\sin(2\tau\omega_L) + 2\omega_L\left(\alpha\tau + \cos(2\tau\omega_L) + 1\right)\right)\Big) \qquad \text{(C.1d)}$$